

Manganese tricarbonyl complexes with asymmetric 2,2-iminopyridine ligands: toward decoupling steric and electronic factors in electrocatalytic CO₂ reduction

Article

Accepted Version

Spall, S. J. P. , Keane, T. , Tory, J. , Cocker, D. C., Adams, H. , Fowler, H. , Meijer, A. J. H. M. , Hartl, F. and Weinstein, J. A. (2016) Manganese tricarbonyl complexes with asymmetric 2,2-iminopyridine ligands: toward decoupling steric and electronic factors in electrocatalytic CO₂ reduction. *Inorganic Chemistry*, 55 (24). pp. 12568-12582. ISSN 0020-1669 doi: <https://doi.org/10.1021/acs.inorgchem.6b01477> Available at <http://centaur.reading.ac.uk/68114/>

It is advisable to refer to the publisher's version if you intend to cite from the work.

To link to this article DOI: <http://dx.doi.org/10.1021/acs.inorgchem.6b01477>

Publisher: American Chemical Society

All outputs in CentAUR are protected by Intellectual Property Rights law, including copyright law. Copyright and IPR is retained by the creators or other copyright holders. Terms and conditions for use of this material are defined in

the [End User Agreement](#).

www.reading.ac.uk/centaur

CentAUR

Central Archive at the University of Reading

Reading's research outputs online

Manganese Tricarbonyl Complexes with Asymmetric 2-Iminopyridine Ligands: Toward Decoupling Steric and Electronic Factors in Electrocatalytic CO₂ Reduction

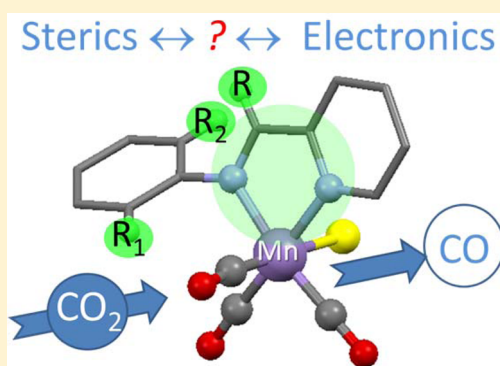
Steven J. P. Spall,[†] Theo Keane,[†] Joanne Tory,[‡] Dean C. Cocker,[†] Harry Adams,[†] Hannah Fowler,[†] Anthony J. H. M. Meijer,^{†,ic} František Hartl,^{*,‡} and Julia A. Weinstein^{*,†,ic}

[†]Department of Chemistry, University of Sheffield, Sheffield S3 7HF, U.K.

[‡]Department of Chemistry, University of Reading, Whiteknights, Reading RG6 6AD, U.K.

S Supporting Information

ABSTRACT: Manganese tricarbonyl bromide complexes incorporating IP (2-(phenylimino)pyridine) derivatives, [MnBr(CO)₃(IP)], are demonstrated as a new group of catalysts for CO₂ reduction, which represent the first example of utilization of (phenylimino)pyridine ligands on manganese centers for this purpose. The key feature is the asymmetric structure of the redox-noninnocent ligand that permits independent tuning of its steric and electronic properties. The α -diimine ligands and five new Mn(I) compounds have been synthesized, isolated in high yields, and fully characterized, including X-ray crystallography. Their electrochemical and electrocatalytic behavior was investigated using cyclic voltammetry and UV–vis–IR spectroelectrochemistry within an OTTLE cell. Mechanistic investigations under an inert atmosphere have revealed differences in the nature of the reduction products as a function of steric bulk of the ligand. The direct ECE (electrochemical–chemical–electrochemical) formation of a five-coordinate anion [Mn(CO)₃(IP)][−], a product of two-electron reduction of the parent complex, is observed in the case of the bulky DIPIMP (2-(((2,6-diisopropylphenyl)imino)methyl)pyridine), TBIMP (2-(((2-*tert*-butylphenyl)imino)methyl)pyridine), and TBIEP (2-(((2-*tert*-butylphenyl)imino)ethyl)pyridine) derivatives. This process is replaced for the least sterically demanding IP ligand in [MnBr(CO)₃(IMP)] (2-((phenylimino)methyl)pyridine) by the stepwise formation of such a monoanion via an ECEC(E) mechanism involving also the intermediate Mn–Mn dimer [Mn(CO)₃(IMP)]₂. The complex [MnBr(CO)₃(IPIMP)] (2-(((2-diisopropylphenyl)imino)methyl)pyridine), which carries a moderately electron donating, moderately bulky IP ligand, shows an intermediate behavior where both the five-coordinate anion and its dimeric precursor are jointly detected on the time scale of the spectroelectrochemical experiments. Under an atmosphere of CO₂ the studied complexes, except for the DIPIMP derivative, rapidly coordinate CO₂, forming stable bicarbonate intermediates, with no dimer being observed. Such behavior indicates that the CO₂ binding is outcompeting another pathway: *viz.*, the dimerization reaction between the five-coordinate anion and the neutral parent complex. The bicarbonate intermediate species undergo reduction at more negative potentials (ca. −2.2 V vs Fc/Fc⁺), recovering [Mn(CO)₃(IP)][−] and triggering the catalytic production of CO.



The interest in solar fuels in terms of both photocatalytic and electrocatalytic CO₂ reduction,¹ in the latter case utilizing sustainable electricity, has been increasing markedly in the new millennium. The recent demonstration of the electrocatalytic activity of manganese² analogues of the archetypal Re(I) catalysts^{3–6} for CO₂ reduction has given a new impetus to research into noble-metal-free catalytic systems. [MnBr(CO)₃(α -diimine)] complexes have been shown to outperform rhenium-based analogues with regard to CO₂ reduction under certain conditions.⁷ Most notably, the presence of a Brønsted acid^{7–10} appears to be a prerequisite for catalysis with a range of tricarbonyl Mn α -diimine complexes.

Mechanistic studies^{5,10} of the active 2,2'-bipyridine-based (R-bpy) manganese catalysts have shown that one-electron reduction of the parent complex [MnBr(CO)₃(R-bpy)]

precursor results in the formation of the Mn–Mn dimer⁵⁰ [Mn(CO)₃(R-bpy)]₂.^{8,9} Notably, neither the primary reduction product [MnBr(CO)₃(R-bpy)^{•−}] nor the five-coordinate radical intermediates [Mn(CO)₃(R-bpy)][•] have been detected by either UV–vis or IR spectroscopy.^{2,7} Nanosecond time-resolved infrared (TRIR) studies reveal that no detectable solvent adduct is formed before the dimerization of Mn species on this time scale; instead, the five-coordinate species is observed, which rapidly dimerizes.¹⁰ For some of the Re analogues, a one-electron-reduced complex, [ReCl(CO)₃(R-bpy)^{•−}], was observed by IR spectroscopy and identified by the ca. 15–20 cm^{−1} decrease in the $\tilde{\nu}(\text{CO})$ energy,^{11–13} as was the 61

Received: June 22, 2016

62 five-coordinate radical $[\text{Re}(\text{CO})_3(\text{tBu-bpy})]^\bullet$ by an additional
63 $15\text{--}20\text{ cm}^{-1}$ shift.

64 Two mechanisms have been proposed^{10,14–18} for the
65 ultimate reduction of $[\text{Mn}(\text{CO})_3(\alpha\text{-diimine})]_2$ in the presence
66 of CO_2 , which can be referred to as the anionic and the
67 oxidative addition¹⁹ pathways. The anionic pathway involves
68 reduction of the dimer $[\text{Mn}(\text{CO})_3(\alpha\text{-diimine})]_2$ at a potential
69 more negative than that of the parent complex, generating the
70 five-coordinate anion $[\text{Mn}(\text{CO})_3(\alpha\text{-diimine})]^-$, to which CO_2
71 coordinates and is catalytically reduced in the presence of a
72 Brønsted acid (the source of H^+). The anionic pathway is
73 broadly similar to the two-electron pathway observed for Re
74 complexes.^{20,21} In contrast, the uncommon second pathway
75 identified using pulsed EPR studies¹⁹ involves coordination of
76 CO_2 to the dimer $[\text{Mn}(\text{CO})_3(2,2'\text{-bpy})]_2$ in the presence of a
77 Brønsted acid in a concerted oxidative addition step. This
78 process is shown to generate a low-spin $\text{Mn}^{\text{II}}\text{--COOH}$ complex,
79 from which CO is subsequently released.

80 Since the catalytic CO_2 reduction with the use of
81 $[\text{MnX}(\text{CO})_3(\alpha\text{-diimine})]$ ($\alpha\text{-diimine} = \text{R-bpy}$; $\text{X} = \text{halide}$ or
82 pseudohalide) has been shown to proceed in many cases via a
83 dimerization step, immobilization of the catalyst²² or
84 introduction of sterically hindering groups at bpy may have a
85 profound effect on the catalytic activity.²³ Indeed, it has
86 recently been shown that the use of bipyridines incorporating
87 bulky groups in the 6,6'-positions^{24,25} (or another bulkier
88 heterocyclic ligand²⁶) largely inhibits dimerization in the
89 catalytic cycle. The result is the formation of the stable five-
90 coordinate anion via the two-electron transfer (ECE) at the first
91 cathodic wave. However, coordination of CO_2 to the five-
92 coordinate anion produces a stable species which must be
93 reduced at considerably more negative potentials²⁷ in order for
94 catalysis to be observed. It has recently been shown that in the
95 presence of a Lewis acid, Mg^{2+} ,^{7,28} the catalytic overpotential²⁹
96 is decreased by approximately 400 mV.

97 A similar behavior was observed for $[\text{MnBr}(\text{CO})_3(\text{R-DAB})]$
98 complexes featuring nonaromatic 1,4-diazabuta-1,3-diene (R-
99 DAB)^{8,9,30} ligands. The reduction potentials of the dimers
100 $[\text{Mn}(\text{CO})_3(\text{R-DAB})]_2$ are almost identical with those of the
101 parent complexes, implying that the five-coordinate anion is
102 produced directly upon reduction and reacts readily with CO_2
103 in solution to form a stable bicarbonate complex^{8,30} and, as
104 with sterically hindered 2,2'-bipyridine ligands,²⁵ a much more
105 negative potential (below 2 V vs Fc/Fc^+) must be applied to
106 trigger catalytic CO_2 reduction. Functionalization of the α -
107 diimine with a sterically bulky group such as ^tBu should also
108 modify the electronic properties of the ligand. In particular, this
109 change should affect the energy of the LUMO, the reduction
110 potential, and catalytic activity.^{23–33}

111 Introducing steric bulk^{23,25} to prevent unwanted reactions of
112 the catalytic species, including dimerization as either Mn–Mn⁹
113 or C(imino)–C(imino) bound species,²¹ while at the same
114 time reducing the risk of increased overpotential is a
115 challenging task. Molecular designs that allow for steric and
116 electronic effects to be decoupled are required.

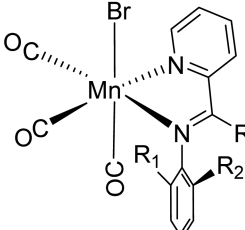
117 In this paper we have investigated a family of tricarbonyl
118 manganese complexes featuring asymmetric α -diimine ligands,
119 iminopyridines (IP).^{21,23,34,35} They combine an accessible
120 $\text{C}=\text{N}$ imino bond of the diazabuta-1,3-diene derivatives
121 DAB³² with the aromatic pyridine part, thereby being a
122 “hybrid” of 2,2'-bipyridine ligands and nonaromatic R-DAB
123 ligands. Each of the parts is important: for instance, a Mn(I)
124 complex with Ph-DAB demonstrates formation of five-

coordinate anions, with the steric bulk of the ligand preventing
dimerization, but does not act as a catalyst for CO_2 reduction
due to insufficiently negative reduction potential.⁸

Introduction of the pyridine moiety allows one to reach the
required reduction potentials, while the Ph group attached to
the $\text{C}=\text{N}$ fragment can be decorated with sterically demanding
substituents, ensuring steric bulk while only slightly affecting
the electronic properties. As the phenyl moiety lies out of plane
with the conjugated α -diimine (because of steric effects), the π
electrons of the phenyl substituent are decoupled from the
metallacycle formed by the metal center and the α -diimine.
Therefore, functionalization of the phenyl ring in the R_1 and R_2
positions with large sterically hindering groups (that also have a
 $+I$ effect) will have only very minimal effects on the electronics
of the active site of the molecule (vide infra). These ligands
offer an opportunity to separate steric and electronic effects in a
chelating α -diimine ligand to a certain extent. Thus, the
possibility arises of a systematic variation of the steric hindrance
by changing R_1 and R_2 groups, while the R group strongly
influences the electronics (but could also hinder the $\text{C}=\text{N}$
bond).

These ligands are readily accessible via simple synthetic
routes, which are suitable for the purpose of comparatively
independent alteration of steric and electronic effects (Chart 1).

Chart 1. General Structure of the Complexes with the Asymmetric α -Diimine Ligands (2- R_1 -6- R_2 -phenyl)(R -imino)pyridine^a



Ligand	R	R_1	R_2
IMP (1)	H	H	H
IPIMP (2)	H	ⁱ Pr	H
DIPIMP (3)	H	ⁱ Pr	ⁱ Pr
TBIMP (4)	H	^t Bu	H
TBIEP (5)	CH_3	^t Bu	H

^aNumbers given in parentheses correspond to the Mn complexes. When $\text{R} = \text{H}$, the ligands will be derivatives of [(phenylimino)methyl]pyridine: IMP ($\text{R}_{1,2} = \text{H}$), IPIMP ($\text{R}_1 = \text{ⁱPr}$, $\text{R}_2 = \text{H}$), and DIPIMP ($\text{R}_{1,2} = \text{ⁱPr}$), TBIMP ($\text{R}_1 = \text{^tBu}$, $\text{R}_2 = \text{H}$). $\text{R} = \text{CH}_3$ gives TBIEP, [((*tert*-butylphenyl)imino)ethyl]pyridine.

The potential of such ligands^{34–38} has been convincingly
illustrated by the recent work on a Re tricarbonyl complex with
2-[[((2-cyclohexyl-1-methyl)methyl)imino]pyridine]³⁶ (both the
one-electron-reduced parent complex and the neutral five-
coordinate $\text{Re}(0)$ species were detected), and Mo pyridine-
monoimides.³⁴

Herein we report a new series of manganese-based catalysts
for CO_2 reduction. We will show that a change in the structure
of the ligands within the same series affects the efficiency of the
process and the relative distribution of the intermediate species,
demonstrating the versatile and tunable nature of these types of
catalysts.

EXPERIMENTAL SECTION

All solvents were supplied by VWR and used as received. The
compounds were purchased from either Sigma-Aldrich or Strem
Chemicals and, unless stated, used as received. Tetrabutylammonium
hexafluorophosphate, $[\text{Bu}_4\text{N}][\text{PF}_6]$, was recrystallized from hot
ethanol and dried overnight in a vacuum oven before use in the
electrochemical studies. TBIEP (2-[[((2-*tert*-butylphenyl)imino)ethyl]-

168 pyridine) and TBIMP were synthesized as previously described;³⁵ the
169 analytical data matched those reported previously. Unless otherwise
170 stated, UV–vis spectra were recorded on a Carry 50 Bio
171 spectrophotometer and IR spectra on a PerkinElmer Spectrum 1
172 FT-IR spectrometer.

173 **Syntheses.** *IMP* (2-[(Phenylimino)methyl]pyridine). Aniline (11.3
174 mmol, 1.05 g, 1.02 mL) was added to 2-pyridinecarboxaldehyde (11.3
175 mmol, 1.2 g, 1.1 mL) in flame-dried glassware and stirred for 1 h.
176 Hexane (10 mL) was added and the solution dried over sodium
177 sulfate. The solution was filtered, concentrated under vacuum, and
178 placed in a freezer overnight. The large yellow needlelike crystals that
179 formed were filtered and washed with hexane. Yield: 73%. ¹H NMR
180 (400 MHz, CDCl₃): δ 8.72 (d, *J* = 4.7 Hz, 1H), 8.61 (s, 1H), 8.21 (d, *J*
181 = 7.9 Hz, 1H), 7.83 (td, *J* = 7.7, 1.6 Hz, 1H), 7.47–7.35 (m, 3H), 7.29
182 (d, *J* = 7.7 Hz, 3H), 1.58 (s, 4H).

183 *IPIMP* (2-[2-((Isopropylphenyl)imino)methyl]pyridine). 2-Isopro-
184 pyraniline (12.4 mmol, 1.7 g, 1.8 mL) was mixed with 2-
185 pyridinecarboxaldehyde (12.4 mmol, 1.3 g, 1.2 mL) in flame-dried
186 glassware and stirred for 1 h. Hexane (20 mL) was added and the
187 solution dried over sodium sulfate. The solution was filtered and
188 solvent removed under vacuum, yielding the product as a brown oil.
189 Previous reports indicated that this compound could not be
190 crystallized; therefore, the oil was used in the next reaction step
191 without further purification (purity by NMR >97%). ¹H NMR (400
192 MHz, CDCl₃): δ 8.72 (ddd, *J* = 4.8, 1.6, 0.9 Hz, 1H), 8.54 (s, 1H),
193 8.26 (dd, *J* = 7.9, 0.9 Hz, 1H), 7.82 (ddd, *J* = 7.9, 1.7, 0.8 Hz, 1H),
194 7.45–7.32 (m, 2H), 7.31–7.22 (m, 2H), 7.08–6.96 (m, 1H), 3.56 (dp,
195 *J* = 13.8, 6.8 Hz, 1H), 1.26 (dd, *J* = 6.8, 4.1 Hz, 7H).

196 *DIPIMP* (2-[(2,6-Diisopropylphenyl)imino)methyl]pyridine). 2,6-
197 Diisopropylaniline (11.3 mmol, 2 g, 2.1 mL) was mixed with 2-
198 pyridinecarboxaldehyde (11.3 mmol, 1.2 g, 1.1 mL) in flame-dried
199 glassware and stirred for 2 h. Hexane (10 mL) was added and the
200 solution dried over sodium sulfate. The solution was filtered and
201 concentrated before being placed in a freezer overnight. Light brown
202 to yellow crystals were formed, which were filtered off and washed
203 with hexane. Yield: 67%. ¹H NMR (400 MHz, CDCl₃): δ 8.73 (ddd, *J*
204 = 4.8, 1.7, 0.9 Hz, 1H), 8.31 (s, 1H), 8.27 (dt, *J* = 7.9, 1.0 Hz, 1H),
205 7.90–7.82 (m, 1H), 7.42 (ddd, *J* = 7.5, 4.9, 1.2 Hz, 1H), 7.22–7.07
206 (m, 3H), 2.97 (hept, *J* = 6.9 Hz, 2H), 1.62 (s, 1H), 1.18 (d, *J* = 6.9 Hz,
207 13H).

208 Complexes 1–6 were prepared from [MnBr(CO)₅] and the
209 corresponding ligand, using diethyl ether as a solvent. The products
210 were collected by centrifugation and washed with diethyl ether to
211 afford analytically pure 1–6. ¹H NMR spectra for 1–5 are given in
212 Figure S122–S126 in the Supporting Information.

213 [MnBr(CO)₃(IMP)] (1). [MnBr(CO)₅] (1.1 mmol, 0.3 g) was
214 combined with IMP (1.1 mmol, 0.2 g) in diethyl ether (20 mL) and
215 refluxed under aerobic conditions for 4 h.³⁹ The product was formed
216 in quantitative yield. ¹H NMR (500 MHz, CDCl₃): δ 9.26 (d, *J* = 5.0
217 Hz, 1H), 8.45 (s, *J* = 27.9 Hz, 1H), 8.14–7.79 (m, 3H), 7.68–7.36 (m,
218 5H). HRMS (TOF-ES, +ve): *m/z* (M + Na⁺) calcd for
219 C₁₅H₁₀N₂O₃NaBrMn 422.9153, found 422.9149.

220 [MnBr(CO)₃(IPIMP)] (2). [MnBr(CO)₅] (0.89 mmol, 0.24 g) was
221 combined with IPIMP (0.89 mmol, 0.2 g) in diethyl ether (20 mL)
222 and refluxed under aerobic conditions for 4 h. The product was
223 formed in quantitative yield. ¹H NMR (500 MHz, CDCl₃): δ 9.27 (s,
224 1H), 8.39 (s, 1H), 8.04 (s, 1H), 7.94 (d, *J* = 4.1 Hz, 1H), 7.78 (d, *J* =
225 7.0 Hz, 1H), 7.61 (s, 1H), 7.48 (d, *J* = 15.3 Hz, 1H), 7.43 (d, *J* = 6.7
226 Hz, 1H), 7.37 (t, 1H), 7.30 (d, *J* = 6.9 Hz, 1H), 3.58 (s, 1H), 3.03 (d, *J*
227 = 35.6 Hz, 1H), 1.47–1.11 (m, 1H). HRMS (TOF-ES, +ve): *m/z* (M
228 + Na⁺) calcd for C₁₈H₁₆N₂O₃NaBrMn 464.9622, found 464.9644.

229 [MnBr(CO)₃(DIPIMP)] (3). [MnBr(CO)₅] (0.75 mmol, 0.2 g) was
230 combined with DIPIMP (0.75 mmol, 0.2 g) in diethyl ether (20 mL)
231 and refluxed under aerobic conditions for 4 h. The product was
232 formed in 97% yield. ¹H NMR (500 MHz, CDCl₃): δ 9.30 (s, 1H),
233 8.41 (s, 1H), 7.99 (d, *J* = 50.7 Hz, 2H), 7.63 (s, 1H), 7.34 (s, 2H), 4.04
234 (s, 1H), 2.91 (s, 1H), 1.34 (d, *J* = 3.1 Hz, 6H), 1.05 (dd, *J* = 80.6, 35.1
235 Hz, 6H). HRMS (TOF-ES, +ve): *m/z* (M + Na⁺) calcd for
236 C₂₁H₂₂N₂O₃NaBrMn 507.0092, found 507.0107.

[MnBr(CO)₃(TBIMP)] (4). [MnBr(CO)₅] (0.84 mmol, 0.23 g) was
237 combined with DIPIMP (0.84 mmol, 0.2 g) in diethyl ether (20 mL)
238 and refluxed under aerobic conditions for 4 h. The product was
239 formed in quantitative yield. ¹H NMR (400 MHz, CDCl₃): δ 9.27 (d, *J* =
240 4.4 Hz, 1H), 8.50 (s, 1H), 8.12 (d, *J* = 6.9 Hz, 1H), 8.03 (t, *J* = 7.2
241 Hz, 1H), 7.91 (d, *J* = 7.1 Hz, 1H), 7.61 (t, *J* = 6.2 Hz, 1H), 7.57 (d, *J* =
242 7.4 Hz, 1H), 7.30 (t, 1H), 1.43 (s, 1H). HRMS (TOF-ESI, +ve): *m/z*
243 (M + Na⁺) calcd for C₁₉H₁₈N₂O₃NaBrMn 478.9774, found 478.9789.

244 [MnBr(CO)₃(TBIEP)] (5). [MnBr(CO)₅] (0.8 mmol, 0.22 g) was
245 combined with TBIEP (0.8 mmol, 0.2 g) and refluxed under aerobic
246 conditions in diethyl ether (20 mL) for 4 h. The product was formed
247 in quantitative yield. ¹H NMR (400 MHz, CDCl₃): δ 9.28 (d, *J* = 5.0
248 Hz, 1H), 8.04 (td, *J* = 7.8, 1.3 Hz, 1H), 7.95 (d, *J* = 7.7 Hz, 1H), 7.88
249 (dd, *J* = 6.1, 3.4 Hz, 1H), 7.65–7.54 (m, 2H), 7.34–7.27 (m, 2H),
250 2.39 (s, 3H), 1.39 (s, 8H). HRMS (TOF-ES, +ve): *m/z* (M + Na⁺)
251 calcd for C₂₀H₂₀N₂O₃NaBrMn 492.9935, found 492.9934.

252 [MnBr(CO)₃(bpy)] (6). This compound was prepared following the
253 literature procedure;² analytical data are in agreement with the
254 literature data. [MnBr(CO)₅] (1.28 mmol, 0.35 g) was combined with
255 2,2'-bipyridine (1.28 mmol, 0.2 g) in diethyl ether (20 mL) and
256 refluxed under aerobic conditions for 4 h. The product was formed in
257 80% yield. ¹H NMR (500 MHz, CDCl₃): δ 9.27 (d, *J* = 4.3 Hz, 1H),
258 8.12 (d, *J* = 6.5 Hz, 1H), 7.99 (t, 1H), 7.53 (t, 1H). HRMS (TOF-ESI,
259 +ve): *m/z* (M + Na⁺) calcd for C₁₃H₈N₂O₃NaBrMn 396.8991, found
260 369.8988.

261 **Cyclic Voltammetry.** Cyclic voltammetry was performed using a
262 Princeton Applied Research VersaSTAT3 potentiostat on 2 mM 1–6
263 in Grubbs dried HPLC-grade acetonitrile containing 2 × 10⁻¹ M
264 [Bu₄N][PF₆] as supporting electrolyte. A glassy-carbon working
265 electrode (surface area 0.07 cm², polished on alumina and paper)
266 and a Pt-wire counter electrode were used with a 0.1 M KCl Ag/AgCl
267 reference electrode.

268 The solutions were deoxygenated by bubbling thoroughly with
269 bottled N₂ (BOC), and the N₂ atmosphere was maintained over the
270 samples during the experiment. To test for catalytic current in the
271 presence of CO₂, the samples were bubbled thoroughly with bottled
272 CO₂ (BOC) and cyclic voltammograms (CVs) were recorded under
273 an atmosphere of CO₂ (some residual water might be present in the
274 CO₂ used to saturate the samples). Water was then added (0.3–6 mL
275 of the solution of each sample) to test the effects of Brønsted acid.
276 Ferrocene was added as the internal standard at the end of all
277 experiments.

278 **Spectroelectrochemistry.** Infrared spectroelectrochemistry was
279 performed using an EmStat3 or EmStat3+ potentiostat (PalmSens,
280 Houten, The Netherlands). The solution of 4 mM complex in the
281 presence of 3 × 10⁻¹ M [Bu₄N][PF₆] in dry acetonitrile was analyzed
282 using an optically transparent thin-layer electrochemical (OTTLE) cell
283 equipped with Pt minigrid working and auxiliary electrodes, an Ag-
284 microwire pseudoreference electrode, and CaF₂ windows. Samples
285 were prepared under an argon atmosphere; for electrocatalytic
286 measurements, the solutions were bubbled with CO₂ on a frit (a
287 few minutes) to saturation under normal pressure. Parallel IR and
288 UV–vis spectral monitoring during the spectroelectrochemical
289 experiment was performed on a Bruker Vertex 70v FT-IR
290 spectrometer or PerkinElmer Spectrum 1 and a Scinco S-3100
291 spectrophotometer, respectively. Thin-layer CVs were recorded in the
292 course of the experiment.

293 **Gas Chromatography Linked to Electrolysis.** Bulk electrolysis
294 was performed on a 0.17 mM solution of each of the complexes in a 60
295 mL solution of acetonitrile/water (9/1 v/v). The cell setup consisted
296 of a Pt-mesh working electrode, a Pt-rod counter electrode in a
297 semiporous compartment, and an Ag-wire pseudoreference electrode
298 in a 0.1 M KCl solution. The potential of the Fc/Fc⁺ recorded in this
299 setup using a glassy-carbon 3 mm diameter electrode was +0.350 V vs
300 Ag wire pseudoreference. Hence, in order to reach the potential
301 necessary for the CO₂ reduction as estimated from the CV data, the
302 potential was held at -1.9 V vs Ag wire for all samples: i.e., -2.25 V vs
303 Fc/Fc⁺. Prior to electrolysis, a CV was recorded in the bulk electrolysis
304 cell using a glassy-carbon working electrode. Gas samples (100 μL)
305 were withdrawn from the head space at regular intervals and analyzed 306

307 by a gas chromatograph fitted with a thermal conductivity detector
308 (Perkin ElmerArnel autosystem XL). H₂ was used as the carrier gas in
309 CO-quantification experiments. N₂ was used as a carrier gas in the
310 control experiment.

311 **X-ray Crystallography.** Crystals were grown using the antisolvent
312 crystallization method, with the solvent dichloromethane and hexane
313 as the antisolvent. Single-crystal X-ray diffraction data were collected
314 on a Bruker SMART APEX-II CCD diffractometer operating a Mo K α
315 sealed-tube X-ray source or a Bruker D8 Venture diffractometer
316 equipped with a PHOTON 100 dual-CMOS chip detector and
317 operating a Cu K α I μ S microfocuss X-ray source. The data were
318 processed using Bruker APEX3 software and corrected for absorption
319 using empirical methods (SADABS) based upon symmetry-equivalent
320 reflections combined with measurements at different azimuthal
321 angles.⁴⁰ The crystal structures were solved and refined using the
322 Bruker SHELXTL software package.

323 **Computational Methods.** Density functional theory (DFT)
324 calculations were performed using the Gaussian 09 program package.⁴¹
325 All calculations utilized the global hybrid exchange correlation
326 functional B3LYP,^{42,43} a “mixed” basis set consisting of the SDD
327 basis set as defined in Gaussian for Mn and the 6-311G(d,p) basis set
328 for all other atoms.^{44–47} The solvent acetonitrile was included using
329 the polarizable continuum model (PCM) as implemented in
330 Gaussian.^{48,49} All species were modeled at the lowest multiplicity
331 appropriate for the electron count, and the restricted formalism was
332 used for closed-shell cases. An “ultrafine” integral grid, as defined by
333 Gaussian, was used and all geometries were confirmed as minima by
334 the absence of imaginary frequencies in their vibrational spectra as
335 calculated within the harmonic approximation. The values of
336 vibrational frequencies have been scaled by 0.966 to match
337 experimental $\nu(\text{CO})$ values of the parent neutral complexes.

338 ■ RESULTS AND DISCUSSION

339 **X-ray Crystallography.** The crystal structures of the
340 complexes [MnBr(CO)₃(α -diimine)] (α -diimine = TBIEP,
341 IMP, IPIMP, DIPIMP) are shown in Figure 1, and selected
342 bond distances and angles are given in Table S11 in the
343 Supporting Information. Similar bond lengths are observed for
344 the four complexes, and these are in good agreement with
345 related [MnBr(CO)₃(α -diimine)] species reported in the
346 literature. The X-ray data are in good agreement with the
347 results obtained through DFT calculations. As predicted by

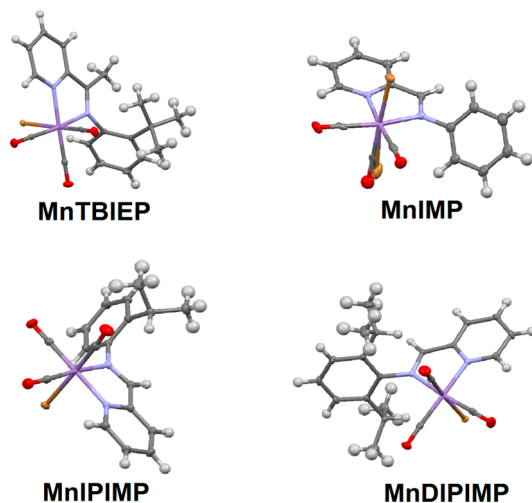


Figure 1. X-ray crystal structures of the studied complexes shown with thermal ellipsoids at the 50% probability level. CCDC 1457930 (MnTBIEP), 1457931 (MnDIPIMP), 1457932 (MnIPIMP), 1457933 (MnIMP). Full crystallographic details are given in the Supporting Information.

DFT, the pyridine and phenyl rings lie approximately 348
orthogonally to one another (dihedral angles between the 349
corresponding planes are MnTBIEP 84.55°, MnIPIMP 83.64°, 350
MnDIPIMP 78°), resulting in little orbital overlap between 351
these two moieties, with the exception of MnIMP, where the 352
two ring systems were significantly less orthogonal (56.54°). 353

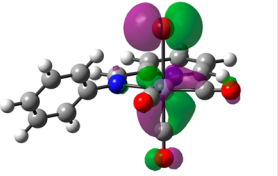
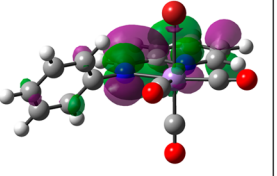
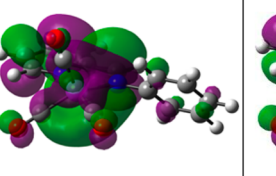
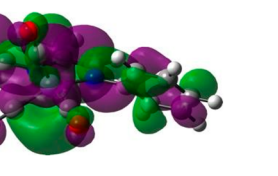
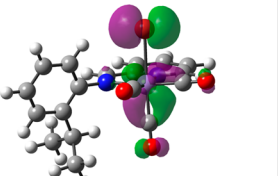
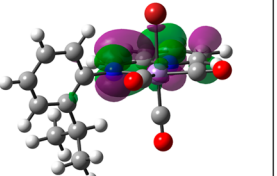
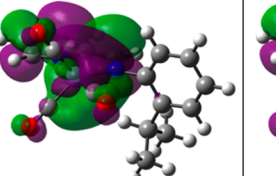
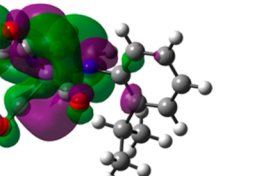
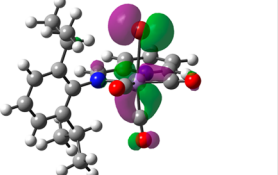
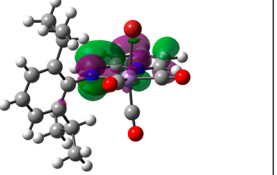
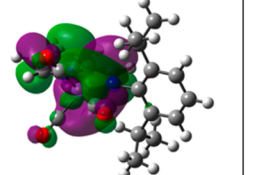
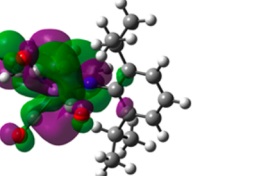
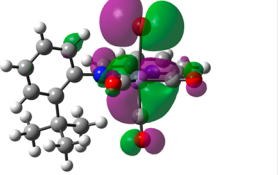
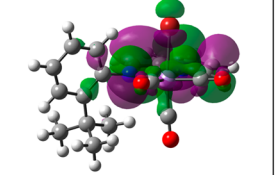
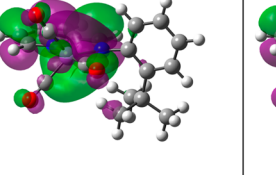
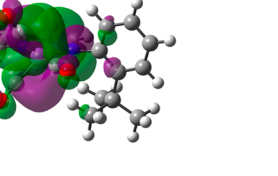
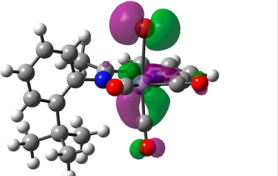
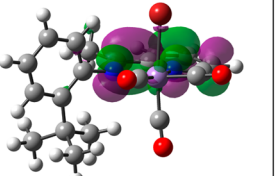
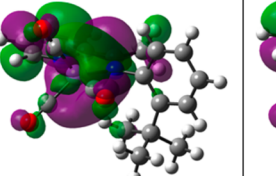
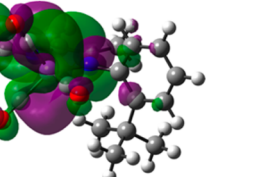
The crystal structures have revealed significant steric 354
hindrance between the substituents R = Me and R₁ = ^tBu in 355
MnTBIEP, which inhibits rotation of the Ph ring and confers 356
conformational rigidity. Rotation of the Ph ring in MnDIPIMP 357
is also inhibited by the two ⁱPr groups and hence also has 358
conformational rigidity. In contrast, MnIMP and MnIPIMP 359
exhibit much smaller steric hindrance, facilitating the rotation of 360
the phenyl ring. 361

**Computational Investigations of Molecular Structures 362
and Frontier Orbitals by DFT.** The optimized geometries of 363
the studied complexes with frontier orbitals overlaid as 364
calculated by DFT are displayed in Table 1. As anticipated, 365
the phenyl group lies out of the plane of the chelating diimine. 366
The HOMO is localized predominantly over the axial Br–Mn– 367
C(O) bonds with almost no contribution from the phenyl 368
moiety. The LUMO resides largely on the imine, pyridyl, and 369
metal center, with minimal contribution from the C1–C2 and 370
C1–C6 σ bonds of the phenyl groups. In the case of MnIMP, 371
due to the lack of substitution at R₁ and R₂, the phenyl moiety 372
is less sterically hindered and thus is positioned closer to the 373
plane of the imino-pyridine fragment, resulting in a small 374
degree of involvement of the phenyl π system in the low-energy 375
unoccupied orbitals. This trend continues in the other low- 376
energy unoccupied orbitals (see Figures S11–S110 in the 377
Supporting Information). 378

The energies of the HOMO in all complexes are within 0.02 379
eV of each other, and all compounds in the IMP subset of 380
complexes have a LUMO that lies within 0.03 eV of those of 381
the other complexes. In contrast, MnTBIEP shows a difference 382
in LUMO energy of +0.19 eV in comparison with IPIMP. This 383
larger difference in LUMO energy comes as result of 384
methylation at the R position. In contrast, adding two isopropyl 385
groups at the R₁ and R₂ positions resulted in an energy 386
difference of just 0.02 eV between MnIMP and MnDIPIMP. 387
The results of the calculations on the trends in the energies of 388
HOMO/LUMO are in full agreement with the experimentally 389
determined redox potentials (see below). These results imply 390
that an almost complete separation between the steric and the 391
electronic effects in the context of few-electron reductions can 392
indeed be achieved in this series of complexes. Changing the R 393
group will strongly affect the energy of the LUMO while also 394
having some impact on the steric properties at the carbon of 395
the imino C=N bond, while changing the R₁ or R₂ groups 396
should have considerable effects on the steric hindrance of the 397
molecule (protecting the Mn and imino-N centers) but hardly 398
affect its electronic properties. 399

The experimental and calculated carbonyl vibrational 400
frequencies of the studied complexes are shown in Table 2. 401
The calculated frequencies are in good agreement with the 402
experimental values. Some systematic discrepancies are 403
apparent: the high-energy A'(1) mode tends to be under- 404
estimated by ~ 10 cm⁻¹, the A'' mode tends to have a lower 405
deviation of only ~ 2 cm⁻¹, and the low-energy A'(2) mode 406
tends to be overestimated by ~ 10 cm⁻¹. It is clear that 407
attachment of the methyl group as R increases the electron 408
density on the metal center and thus also the Mn to CO π 409
back-bonding, as evidenced by the smaller values of $\nu(\text{CO})$ for 410

Table 1. Frontier Orbitals of the Complexes 1–5 and the Corresponding Five-Coordinate Anions Calculated at the B3LYP/SDD+6-311G(d,p)/IEFPCM Level^a

HOMO	LUMO	HOMO	LUMO
Parent Complex		Five-coordinate anion	
MnIMP		MnIMP	
 $\epsilon = -6.31 \text{ eV}$	 $\epsilon = -2.84 \text{ eV}$	 $\epsilon = -3.67 \text{ eV}$	 $\epsilon = -1.18 \text{ eV}$
MnIPIMP		MnIPIMP	
 $\epsilon = -6.33 \text{ eV}$	 $\epsilon = -2.81 \text{ eV}$	 $\epsilon = -3.70 \text{ eV}$	 $\epsilon = -1.01 \text{ eV}$
MnDIPIMP		MnDIPIMP	
 $\epsilon = -6.31 \text{ eV}$	 $\epsilon = -2.83 \text{ eV}$	 $\epsilon = -3.67 \text{ eV}$	 $\epsilon = -0.99 \text{ eV}$
MnTBIMP		MnTBIMP	
 $\epsilon = -6.36 \text{ eV}$	 $\epsilon = -2.80 \text{ eV}$	 $\epsilon = -3.64 \text{ eV}$	 $\epsilon = -1.02 \text{ eV}$
MnTBIEP		MnTBIEP	
 $\epsilon = -6.31 \text{ eV}$	 $\epsilon = -2.84 \text{ eV}$	 $\epsilon = -3.67 \text{ eV}$	 $\epsilon = -1.18 \text{ eV}$

^aIsovalue of 0.04 ($e \text{ bohr}^{-3}$)^{1/2}.

MnTBIEP in comparison to the IMP subseries (complexes 1–4). However, substitution at R₁ and R₂ has only a slight effect on the frequencies. It should be noted that the magnitude of these effects is small ($<10 \text{ cm}^{-1}$) and that it is beyond the scope of this computational work to unravel the various factors effecting changes in CO stretching frequencies.⁵⁰

The results of DFT calculations (Table 2) of IR spectra for the parent Br complexes $[\text{MnBr}(\text{CO})_3(\alpha\text{-diimine})]$ (1–5) and the corresponding $[\text{Mn}(\text{CO})_3(\text{H}_2\text{O})(\alpha\text{-diimine})]^+$ (cationic

aquo complexes) match the experimental data well. We therefore use the calculated $\nu(\text{CO})$ wavenumbers for the hydrolyzed aquo and reduced (dimer and anion) species to aid the analysis of the IR spectra and product assignment in the course of the corresponding cathodic IR-SEC experiments (vide infra).

Adding electron-donating groups (iPr, tBu) to the phenyl ring of the IMP subseries does not have a large effect on the $\nu(\text{CO})$ frequency, the band positions being virtually unchanged

Table 2. Experimentally Obtained and Calculated Frequencies of Carbonyl Stretching Vibrations, $\nu(\text{CO})$, of the Mn Complexes in Their Neutral Form (1–5) and Transient One-Electron-Reduced Form, as well as Five-Coordinate Anion, a Cationic Aqua Complex, and an Mn–Mn Bound Dimer^a

species	$\nu(\text{CO})/\text{cm}^{-1}$	
	calcd	exptl
[MnBr(CO) ₃ (IMP)] (1)	2020, 1943, 1931	2029, 1941, 1926
[MnBr(CO) ₃ (IMP)] ⁻	1992, 1906, 1897	not obsd
[Mn(CO) ₃ (H ₂ O)(IMP)] ⁺	2046, 1966, 1957	2051, 1964, 1958 ^b
[Mn(CO) ₃ (IMP)] ⁻	1906, 1830, 1813	1930, 1826
[Mn(CO) ₃ (IMP)] ₂	1964, 1918, 1891, 1882, 1872, 1868	1994, 1949, 1902, 1875
[MnBr(CO) ₃ (IPIMP)] (2)	2020, 1945, 1929	2029, 1943, 1923
[MnBr(CO) ₃ (IPIMP)] ⁻	1988, 1905, 1891	not obsd
[Mn(CO) ₃ (H ₂ O)(IPIMP)] ⁺	2044, 1963, 1956	2049, 1959 (br)
[Mn(CO) ₃ (IPIMP)] ⁻	1905, 1826, 1808	1929, 1824
[Mn(CO) ₃ (IPIMP)] ₂	1964, 1917, 1890, 1881, 1866, 1860	1981, 1949, 1901, 1882, 1862
[MnBr(CO) ₃ (DIPIMP)] (3)	2019, 1945, 1929	2028, 1944, 1922
[MnBr(CO) ₃ (DIPIMP)] ⁻	1985, 1906, 1890	not obsd
[Mn(CO) ₃ (H ₂ O)(DIPIMP)] ⁺	2045, 1964, 1957	2050, 1960 (br) ^b
[Mn(CO) ₃ (DIPIMP)] ⁻	1903, 1824, 1806	1929, 1829/1822
[Mn(CO) ₃ (DIPIMP)] ₂	1965, 1918, 1890, 1880, 1860, 1850	not obsd
[MnBr(CO) ₃ (TBIMP)] (4)	2020, 1947, 1925	2029, 1945, 1923
[MnBr(CO) ₃ (TBIMP)] ⁻	1988, 1907, 1890	not obsd
[Mn(CO) ₃ (H ₂ O)(TBIMP)] ⁺	2045, 1965, 1956	not obsd
[Mn(CO) ₃ (TBIMP)] ⁻	1906, 1827, 1807	1928, 1823
[Mn(CO) ₃ (TBIMP)] ₂	1964, 1916, 1889, 1879, 1862, 1854	not obsd
[MnBr(CO) ₃ (TBIEP)] (5)	2018, 1944, 1921	2028, 1943, 1917
[MnBr(CO) ₃ (TBIEP)] ⁻	1980, 1904, 1883	not obsd
[Mn(CO) ₃ (H ₂ O)(TBIEP)] ⁺	2042, 1962, 1950	2048, 1960, 1954
[Mn(CO) ₃ (TBIEP)] ⁻	1897, 1819, 1798	1922, 1814 (br)
[Mn(CO) ₃ (TBIEP)] ₂	1958, 1909, 1880, 1870, 1850, 1841	not obsd

^aIn acetonitrile at 293 K. ^bPositions are approximate, as the parent CO stretching vibrations obscure those of the cationic aqua complex.

The UV–vis absorption spectra (Figure 2) are consistent with the nature of the frontier orbitals obtained from the

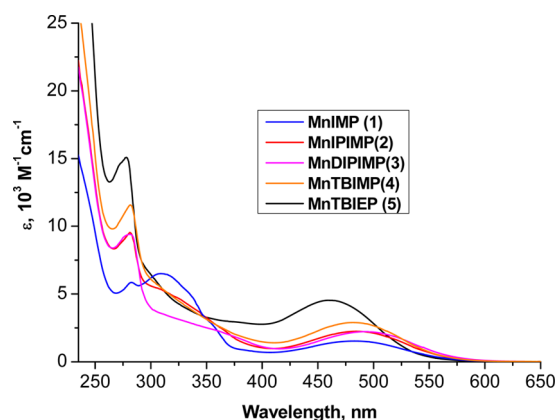


Figure 2. Electronic absorption spectra of the manganese complexes 1–5 studied in this work, in DCM at 293 K.

calculated data. The lowest energy absorption band for the complexes of the IMP subseries 1–4 occurs at approximately the same ca. 500 nm position. In contrast MnTBIEP (5) exhibits an absorption band with a maximum at a shorter wavelength, 460 nm, due to electron donation from the Me group which destabilizes the LUMO.

Cyclic Voltammetry. Electrochemical studies showed significant differences between the cathodic path of MnTBIEP (5) and those of the IMP subseries (1–4).

Under an N₂ atmosphere, [MnBr(CO)₃(TBIEP)] shows a single reduction wave at $E_{p,c} = -1.53$ V and an intense anodic wave at $E_{p,a} = -1.3$ V observed on the reverse anodic scan. This behavior is similar to that of [MnBr(CO)₃(ⁱPr-DAB)] (ⁱPr-DAB = 1,4-diisopropyl-1,4-diazabuta-1,3-diene),⁸ which is reduced by an ECE mechanism. The initial one-electron reduction results in dissociation of the bromide to form a five-coordinate radical, [Mn(CO)₃(TBIEP)][•], which is concomitantly reduced to the five-coordinate anion [Mn(CO)₃(TBIEP)]⁻ (reoxidized at -1.3 V) at the potential required for the reduction of [MnBr(CO)₃(TBIEP)]. A small anodic wave at -0.6 V is characteristic of oxidation of [Mn(CO)₃(TBIEP)]₂ formed in the course of the anodic path of the five-coordinate anion, and indicates that dimerization can still occur with R = CH₃. The dimer could also be produced in a reaction of [Mn(CO)₃(TBIEP)]⁻ with neutral [MnBr(CO)₃(TBIEP)] on the cathodic scan, but the absence of a cathodic wave for reduction of [Mn(CO)₃(TBIEP)]₂ indicates that its reduction potential is too close to that of [MnBr(CO)₃(TBIEP)] for a separate reduction wave to be observed.

The CV traces of MnIMP obtained under an N₂ atmosphere show three cathodic reduction peaks at $E_{p,c} = -1.28$, -1.41 , and -1.54 V and a strong anodic peak at $E_{p,a} = -1.24$ V. The first reduction at -1.28 V can be assigned to the cation [Mn(CO)₃(H₂O)(IMP)]⁺; it is likely that the peak at -1.41 V is due to remaining nonhydrolyzed [MnBr(CO)₃(IMP)] or a solvent adduct,¹¹ while the -1.54 V wave corresponds to the reduction of the dimeric species (see also the IR spectroelectrochemical section below). The five-coordinate anion [Mn(CO)₃(IMP)]⁻ is probably the reduction product at all three different cathodic waves (the parent complex [MnBr(CO)₃(IMP)], aquo complex, and the IMPMn–MnIMP

among complexes 1–4. The two higher-frequency bands are at 2028–2029 and 1943–1944 cm⁻¹ for all five complexes, while the lowest $\nu(\text{CO})$ band is seen at 1923–1922 cm⁻¹ for the IMP series but is shifted to lower energy, 1917 cm⁻¹ in [MnBr(CO)₃(TBIEP)], where the increased π back-donation is caused by R = Me. This invariability of $\nu(\text{CO})$ frequencies, while the dihedral angles between the planes of the pyridine and phenyl moieties of the IP ligands are clearly changing drastically, from ~ 56 to $\sim 84^\circ$, confirms the opportunity of the somewhat independent tuning of electronic and steric factors. Calculations performed on the five-coordinate anions of the studied compounds, [Mn(CO)₃(diimine)]⁻, show trends very similar to what has been observed in the parent complexes. Both the HOMO and LUMO are predominantly delocalized over the tricarbonyl-Mn and α -diimine metallacycle, with little participation from the phenyl ring, with the exception of MnIMP, the LUMO of which has a significant contribution from the phenyl moiety.

491 dimer), as evidenced by its anodic wave at $E_{p,a} = -1.24$ V on
 492 the reverse anodic scan (accompanied by the dimer oxidation
 493 above -0.5 V).

494 Over time a smaller cathodic wave emerges at $E_{p,c} = -1.35$ V,
 495 due to the aquo-coordinated cationic complex forming via
 496 hydrolysis of the parent Br complex (see Figures S111 and S112
 497 in the Supporting Information). Under an atmosphere of CO_2
 498 the anodic wave of $[\text{Mn}(\text{CO})_3(\text{TBIEP})]^-$ at -1.3 V disappears,
 499 and the profile of the CV also changes (Figure 3), with a broad

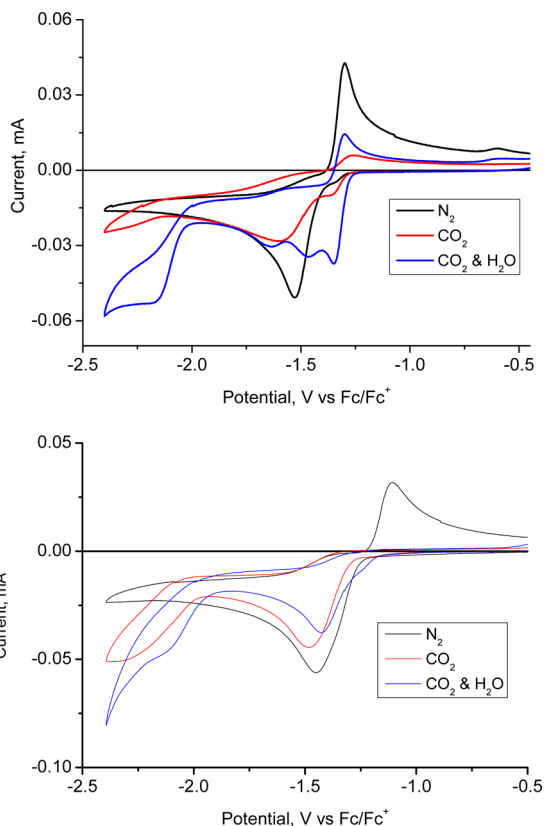


Figure 3. Cyclic voltammograms of 1 mM MnTBIEP (top panel) and MnTBIMP (bottom panel) in acetonitrile with 0.2 M $[\text{Bu}_4\text{N}][\text{PF}_6]$ as supporting electrolyte, under a N_2 atmosphere (black), CO_2 atmosphere (red), and CO_2 with 4.7% added water (blue) at a scan rate of 0.1 V s^{-1} .

500 cathodic wave of $[\text{MnBr}(\text{CO})_3(\text{TBIEP})]$ shifted slightly
 501 negatively, indicating an interaction with CO_2 . However,
 502 similar to the case for Mn-bpy complexes,² catalytic reduction
 503 of CO_2 in the absence of a Brønsted acid was not observed (the
 504 small peak beginning around -2.18 V is due to a small amount
 505 of water entering the CV cell when it is being saturated with
 506 CO_2). Addition of 0.3 mL of water leads to significant current
 507 enhancement at -2.18 V, in line with what has been observed
 508 with $[\text{MnBr}(\text{CO})_3(\text{iPr-DAB})]$.⁸

509 Under a CO_2 atmosphere, the increased cathodic current is
 510 seen at ~ -2.2 V for all complexes. We believe this is due to
 511 some amount of the bicarbonate complex being formed, likely
 512 due to traces of water in the CO_2 used.³³ When 10% water is
 513 added to the CO_2 -saturated solution, a strong current
 514 enhancement is observed at -2.21 V. Importantly, CVs
 515 recorded under a N_2 atmosphere in acetonitrile in the presence
 516 of water do not show catalytic current enhancement (see
 517 Figures S114–S118 in the Supporting Information); thus, both

CO_2 and water are required for the current enhancement to be
 518 observed. 519

Under a CO_2 atmosphere, no anodic wave corresponding to
 520 reoxidation of the five-coordinate anion is observed for the least
 521 sterically hindered $[\text{Mn}(\text{CO})_3(\text{IMP})]^-$ (Figure 4) or for the
 522 523

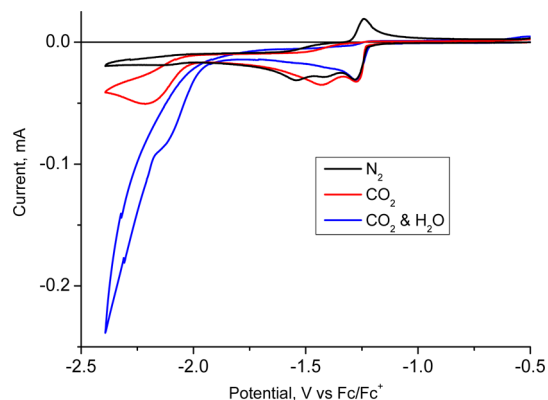


Figure 4. Cyclic voltammograms of 1 mM MnIMP in acetonitrile with 0.2 M $[\text{Bu}_4\text{N}][\text{PF}_6]$ at a scan rate of 0.1 V s^{-1} , under an atmosphere of N_2 (black), CO_2 (red), and CO_2 with 4.7% H_2O (blue).

monosubstituted complexes **2** and **4**, a behavior indicative of a
 523 rapid reaction of the anion with CO_2 . A diminished but clear
 524 anodic wave of $[\text{Mn}(\text{CO})_3(\text{TBIEP})]^-$ can be observed under a
 525 CO_2 vs a N_2 atmosphere (Figure 3), suggesting that
 526 $[\text{Mn}(\text{CO})_3(\text{TBIEP})]^-$ associates with CO_2 less efficiently.
 527 While, similarly to MnIPIMP, no anodic wave corresponding
 528 to $[\text{Mn}(\text{CO})_3(\text{TBIMP})]^-$ reoxidation under a CO_2 atmosphere
 529 could be observed, indicating that CO_2 association is rapid, the
 530 overall current enhancement for this complex is comparatively
 531 low, indicating lower efficiency at reducing CO_2 , perhaps due to
 532 the bicarbonate intermediate somewhat preventing the recovery
 533 of the five-coordinate catalytic species. 534

Under N_2 , reduction of $[\text{MnBr}(\text{CO})_3(\text{IPIMP})]$ is seen at $E_{p,c}$
 535 -1.49 V, accompanied by a wave at $E_{p,c} = -1.29$ V, assigned to
 536 the cationic aqua complex $[\text{Mn}(\text{CO})_3(\text{H}_2\text{O})(\text{IPIMP})]^+$ (Figure
 537 5). As discussed above, upon addition of CO_2 the oxidation
 538 539 wave of the anion $[\text{Mn}(\text{CO})_3(\text{IPIMP})]^-$ is not observed,
 540 indicating a rapid reaction between the five-coordinate anion

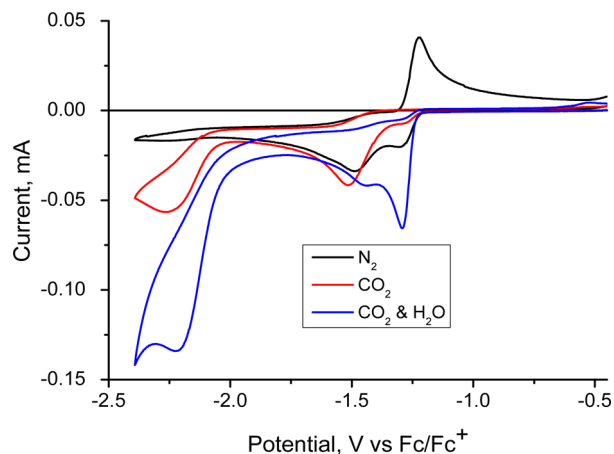


Figure 5. Cyclic voltammograms of 1 mM MnIPIMP in acetonitrile with 0.2 M $[\text{Bu}_4\text{N}][\text{PF}_6]$ at a scan rate of 0.1 V s^{-1} , under an atmosphere of N_2 (black), CO_2 (red), and CO_2 with 4.7% H_2O (blue).

541 and CO₂. Some current enhancement at -2.26 V is observed
 542 upon saturation with CO₂, which is enhanced greatly upon the
 543 addition of 0.3 mL of water (the current enhancement
 544 corresponds to the cathodic wave of the bicarbonate complex,
 545 identified in the IR spectra (vide infra): some catalysis occurs
 546 due to hydrolysis caused for example by residual water in the
 547 electrolyte or in the CO₂).

548 CV of MnTBIMP (Figure 3, bottom panel) is similar to that
 549 of MnIPIMP and MnTBIEP with a strong cathodic wave at
 550 -1.45 V. At ca. -2.28 V current enhancements ascribed to CO₂
 551 reduction can be observed under CO₂ and CO₂ with added
 552 H₂O, though the *i*_{cat}/*i*_p values (Table S11 in the Supporting
 553 Information) are somewhat lower in comparison to the other
 554 complexes studied here. Importantly, the anodic wave of the
 555 five-coordinate anion reoxidation is not detected for MnIPIMP
 556 and MnTBIMP but is clearly seen for slower reacting
 557 MnTBIEP and MnDIPIMP anions.

558 MnDIPIMP shows significant differences in the CV traces in
 559 comparison to the other complexes of the IMP subseries
 560 (Figure 6). Similarly to the IMP and IPIMP complexes, a

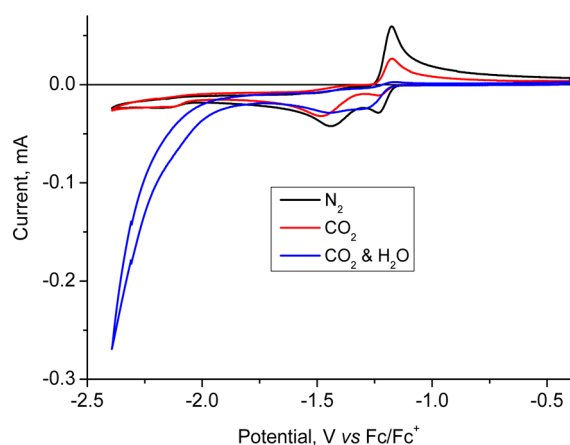


Figure 6. Cyclic voltammograms of 1 mM MnDIPIMP in acetonitrile with 0.2 M [Bu₄N][PF₆] at a scan rate of 0.1 V s⁻¹, under an atmosphere of N₂ (black), CO₂ (red), and CO₂ with 4.7% H₂O (blue).

561 formation of an aqua cation complex ([Mn(CO)₃(H₂O)-
 562 (DIPIMP)]⁺) is observed in solution. However, upon
 563 saturation with CO₂ no additional processes (intermediate
 564 bicarbonate complex reduction) or current enhancement below
 565 -2 V is observed and the anodic peak due to oxidation of
 566 [Mn(CO)₃(DIPIMP)]⁻ does not fully disappear. This suggests
 567 that the reduced complex is less prone to interact with CO₂, as
 568 would be expected due to the increased steric hindrance and
 569 structural rigidity of the complex arising from the two ^tPr
 570 substituents at the N-phenyl rings.

571 **IR and UV-Vis Spectroelectrochemistry under an
 572 Inert Atmosphere.** IR spectroscopy²⁰ is an ideal tool to
 573 monitor the cathodic processes in the studied complexes, due
 574 to presence of the carbonyl ligands as strong IR reporters.
 575 Table 2 gives the key experimental and calculated vibrational
 576 frequencies for the starting complexes and several relevant
 577 intermediate and dimer species. IR spectroelectrochemistry
 578 (IR-SEC) was used to probe the intermediates produced upon
 579 reduction and to monitor their presence during CO₂ reduction.

580 IR spectra of MnTBIEP (Figure 7) show, upon the first
 581 reduction, depletion of the parent $\nu(\text{CO})$ bands, with new
 582 bands growing in at 1922 and 1898 cm⁻¹ and a broad feature at

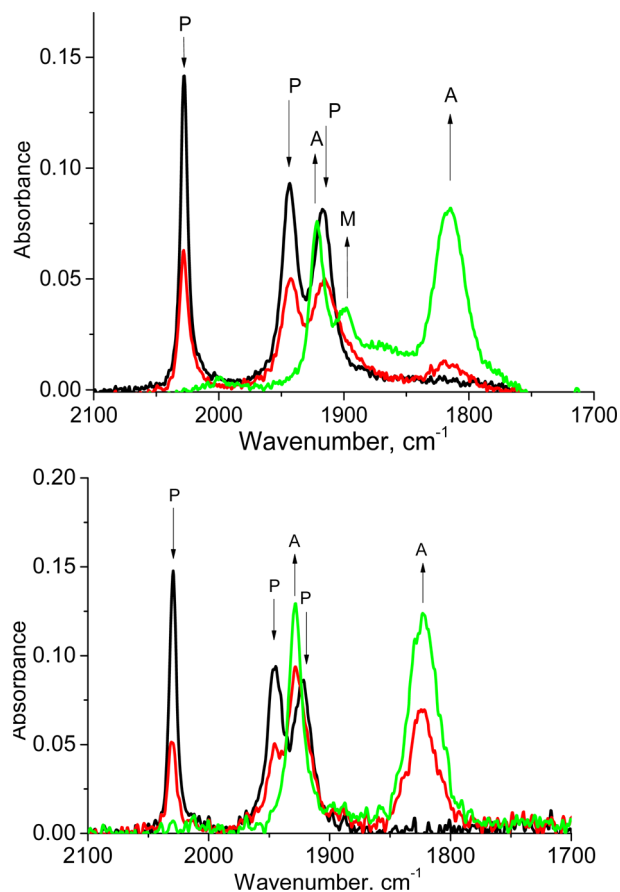


Figure 7. IR spectral changes accompanying in situ reduction of complexes in Ar-saturated acetonitrile/0.2 M [Bu₄N][PF₆] within an OTTE cell. (top) For MnTBIEP, a direct reduction of the parent complex (black line) to the five-coordinate anion (green line) is observed. (P) [MnBr(CO)₃(TBIEP)]; (A) [Mn(CO)₃(TBIEP)]⁻; (M) an unassigned side product. (bottom) For MnTBIMP, a direct reduction of the parent complex (black line) to the five-coordinate anion (green line) is observed: (P) [MnBr(CO)₃(TBIMP)]; (A) [Mn(CO)₃(TBIMP)]⁻.

1814 cm⁻¹. The bands at 1922 and 1814 cm⁻¹ can be assigned
 583 to the five-coordinate anion [Mn(CO)₃(TBIEP)]⁻, an assign-
 584 ment supported by DFT calculations. The band at 1898 cm⁻¹,
 585 which grows in after the five-coordinate anion begins to form,
 586 could tentatively be attributed to a decomposition product.
 587 UV-vis spectroelectrochemistry (Figure S113 in the Support-
 588 ing Information) supports this notion, as only a band at ca. 570
 589 nm has been detected, which corresponds to the five-
 590 coordinate anion. Differently from the MnIMP and MnIPIMP
 591 complexes (see below), there is no indication of dimer
 592 ([Mn(CO)₃(TBIEP)]₂) formation during the reduction of
 593 MnTBIEP on the time scale of the experiments performed.

594 MnTBIMP mirrors the behavior of MnTBIEP with the bands
 595 at 2029, 1945, and 1923 cm⁻¹ corresponding to the parent
 596 complex being replaced concertedly with bands at 1928 and
 597 1823 cm⁻¹ corresponding to the five-coordinate anion, with no
 598 intermediate species being observed. This would suggest that
 599 the direct formation of the five-coordinate anion is due to the
 600 steric demands of the ^tBu group, since the mono-^tPr derivative
 601 2 does exhibit dimer formation (Table 1).
 602

The results of the IR-SEC study of MnIMP are shown in
 603 Figure 8. The first reduction of MnIMP in CH₃CN under an Ar
 604 atmosphere is accompanied by depletion of the parent IR bands
 605

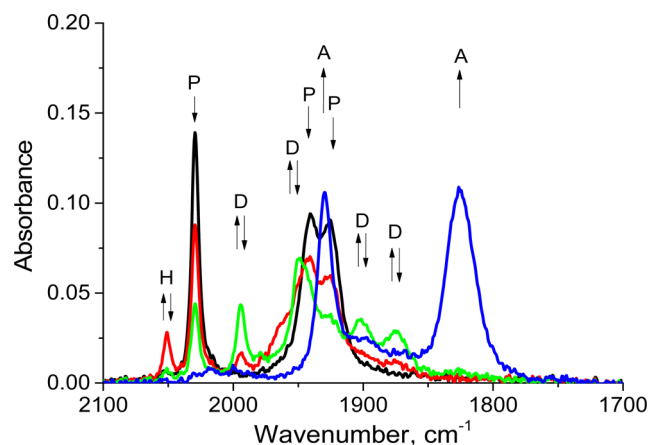


Figure 8. IR spectral changes accompanying in situ reduction of MnIMP in Ar-saturated acetonitrile/0.2 M $[\text{Bu}_4\text{N}][\text{PF}_6]$ within an OTTLE cell. The parent complex $[\text{MnBr}(\text{CO})_3(\text{IMP})]$ (P, black line), and aquo cation $[\text{Mn}(\text{CO})_3(\text{H}_2\text{O})(\text{IMP})]^+$ (H, additional features in the red spectrum) are reduced to the dimer $[\text{MnBr}(\text{CO})_3(\text{IMP})]_2$ (D, green line) followed by reduction of the dimer to the five-coordinate anion $[\text{Mn}(\text{CO})_3(\text{IMP})]^-$ (A, blue line). The intermediate spectrum (red line) recorded between those of the parent complex and the dimer also shows the features of the aquo complex.

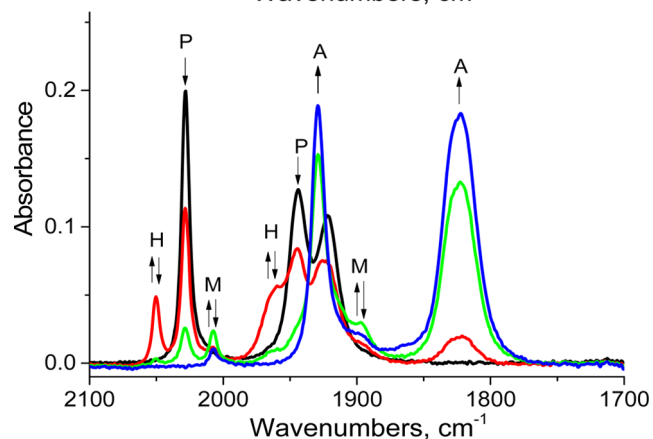
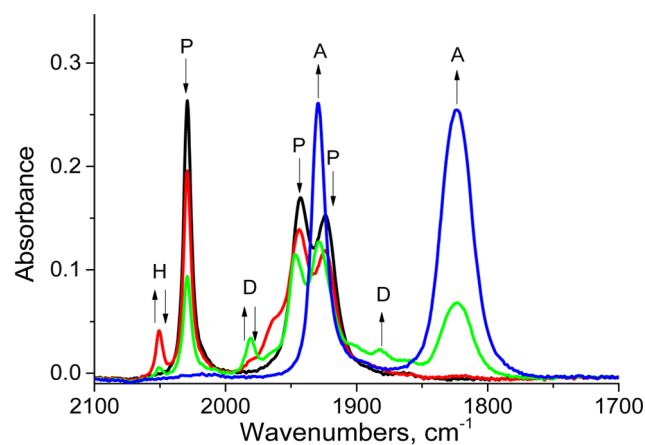


Figure 9. IR spectral changes accompanying in situ reduction of the complexes in Ar-saturated acetonitrile/0.2 M $[\text{Bu}_4\text{N}][\text{PF}_6]$ within an OTTLE cell. (top) MnIPIMP, with concurrent formation of a dimer and a five-coordinate anion on reduction of the parent complex being observed: (P) $[\text{MnBr}(\text{CO})_3(\text{IPIMP})]$; (D) $[\text{Mn}(\text{CO})_3(\text{IPIMP})]_2$; (A) $[\text{Mn}(\text{CO})_3(\text{IPIMP})]^-$; (H) $[\text{Mn}(\text{CO})_3(\text{H}_2\text{O})(\text{IPIMP})]^+$. (bottom) MnDIPIMP, with reduction of the parent complex to a five-coordinate anion being observed: (P) $[\text{MnBr}(\text{CO})_3(\text{DIPIMP})]$; (A) $[\text{Mn}(\text{CO})_3(\text{DIPIMP})]^-$; (H) $[\text{Mn}(\text{CO})_3(\text{H}_2\text{O})(\text{DIPIMP})]^+$; (M) $[\text{Mn}(\text{CO})_3(\text{MeCN})(\text{DIPIMP})]^*$.

606 at 2029, 1941, and 1926 cm^{-1} . Simultaneously, the growth of
 607 new bands at 1994, 1949, 1902, and 1875 cm^{-1} is seen, which
 608 are characteristic of the Mn–Mn dimer^{8,9,13,30} $[\text{Mn}-$
 609 $(\text{CO})_3(\text{IMP})]_2$. Additionally, a peak at 2051 cm^{-1} grows in
 610 initially, which is assigned to the intermediate aqua cation
 611 $[\text{Mn}(\text{CO})_3(\text{H}_2\text{O})(\text{IMP})]^+$ observed also by cyclic voltammetry.
 612 Further reduction of the dimer leads to formation of broad
 613 absorption bands at 1826 and 1930 cm^{-1} , once the formation of
 614 the dimer species is complete. These features are characteristic
 615 of the formation of the five-coordinate anion^{8,9,13} $[\text{Mn}-$
 616 $(\text{CO})_3(\text{IMP})]^-$. UV–vis spectroelectrochemistry performed
 617 in parallel with the IR–SEC experiment confirms the presence
 618 of both of these species (Figure S114 in the Supporting
 619 Information) via the broad absorption band at ca. 800 nm
 620 (assigned to the dimer) and the intense absorption at ca. 675
 621 nm (assigned to the five-coordinate anion).⁸ All complexes in
 622 the IMP subseries exhibited a small transient peak at ca. 2050
 623 cm^{-1} upon reduction. This is assigned to the aquo complex
 624 $[\text{Mn}(\text{CO})_3(\text{H}_2\text{O})(\text{IMP})]^+$.

625 Differently from MnIMP, MnIPIMP showed concurrent
 626 formation of the dimer and the five-coordinate anion upon
 627 reduction of the parent complex (Figure 9, top). The
 628 introduction of the isopropyl substituent at the phenyl ring
 629 leads to the observation of a small amount of the five-
 630 coordinate anion $[\text{Mn}(\text{CO})_3(\text{IPIMP})]^-$ (absorbing at 1929 and
 631 1824 cm^{-1}), which grows in alongside peaks indicative of dimer
 632 formation (1981, 1949, 1901, 1882, and 1862 cm^{-1}).

633 Importantly, the IR absorption bands, corresponding to both
 634 the dimer and the five-coordinate anion, grew in simulta-
 635 neously. UV–vis spectroelectrochemistry confirmed the
 636 presence of both dimer and five-coordinate species in this
 637 case, as is evident from Figure S113 in the Supporting
 638 Information).

639 In contrast, only the five-coordinate anion is detected already
 640 from the onset of the reduction of MnDIPIMP under the
 641 experimental conditions used. In this case, there is no evidence
 642 for the dimer formation during the reduction of the parent
 643 complex. As shown in Figure 9 (bottom), an intense peak at

1823 cm^{-1} , assigned to the five-coordinate anion, grew in,
 followed closely by smaller peaks at 2007 and 1899 cm^{-1} . The
 second peak assigned to the five-coordinate anion at 1929 cm^{-1}
 was masked by the absorption of the parent complex at the
 beginning of the reduction process. We tentatively assign the
 peaks at 2007/1899 cm^{-1} to the solvent-coordinated radical
 species $[\text{Mn}(\text{CO})_3(\text{MeCN})(\text{DIPIMP})]^*$, in analogy with
 $[\text{Re}(\text{CO})_3(\text{PrCN})(^i\text{Pr-PyCa})]^{17}$ ($^i\text{Pr-PyCa}$ = (isopropylimino)-
 pyridine; PrCN = butyronitrile) which shows $\nu(\text{CO})$ bands at
 2005 and 1885 (br) cm^{-1} . Further, since the anodic wave of the
 dimer oxidation is not observed in the CV of MnDIPIMP, but a
 reduced radical species is observed in IR–SEC, it is evident
 that the DIPIMP ligand prevents dimerization.

MnTBIMP shows behavior intermediate to that of
 MnTBIEP and MnIPIMP: similarly to MnTBIEP, the ^iBu
 substituent prevent dimer formation upon reduction. However,
 differently from MnTBIEP, and similar to MnIPIMP, a rapid
 reaction with CO_2 takes place, which in the case of MnTBIEP is
 considerably slowed by the R = Me group. It is important to
 note that if Mn–Mn dimer is reduced at the same or even less
 negative potentials than that of the parent complex, it will not
 be detected in the studies.⁹ Thus, the comments above

666 regarding the absence of dimer formation only relate to the Br
 667 complexes studied here. Substituting Br⁻ with a different group,
 668 which would lead to the parent complex being reduced at less
 669 negative potentials, may permit detection of these species. Five-
 670 coordinate complex formation appears to correlate with a less
 671 negative first reduction potential (see Table 3). A comparable

Table 3. Cathodic Potentials (V, vs Fc/Fc⁺) of the Parent Complexes [MnBr(CO)₃(IP)] (1 mM, Acetonitrile, 0.2 M [Bu₄N][PF₆]) and Corresponding Cationic Mn Aquo Derivatives Formed in Situ by Partial Hydrolysis

complex	$E_{p,c}$	catalytic potential ^b
[MnBr(CO) ₃ (IMP)] (1)	-1.41, -1.54 ^a	-2.21
[Mn(CO) ₃ (H ₂ O)(IMP)] ⁺	-1.28	
[MnBr(CO) ₃ (IPIMP)] (2)	-1.49	-2.26
[Mn(CO) ₃ (H ₂ O)(IPIMP)] ⁺	-1.29	
[MnBr(CO) ₃ (DIPIMP)] (3)	-1.44	-2.16
[Mn(CO) ₃ (H ₂ O)(DIPIMP)] ⁺	-1.23	
[MnBr(CO) ₃ (TBIMP)] (4)	-1.45	~-2.28
[MnBr(CO) ₃ (TBIEP)] (5)	-1.53	-2.18
[Mn(CO) ₃ (H ₂ O)(TBIEP)] ⁺	-1.35	

^aThis process probably corresponds to a reduction of the dimer.

^bLargely coinciding with the reduction of a bicarbonate complex (see the spectroelectrochemical section).

672 correlation was found for Mn-R-DAB complexes and sterically
 673 hindered 2,2'-bipyridines already reported in the literature.
 674 These complexes also exhibit less negative first reduction
 675 potentials in comparison to their less sterically hindered
 676 counterparts and form five-coordinate anions directly upon
 677 reduction.^{8,25}

678 **IR and UV-Vis Spectroelectrochemistry under a CO₂**
 679 **Atmosphere.** Electrochemical behavior under a CO₂ atmo-
 680 sphere is vastly different from that under a N₂ or Ar atmosphere.
 681 The electrocatalytic reduction of CO₂ with the four Mn
 682 complexes can be described in terms of three different types of
 683 behavior, largely controlled by the steric hindrance of the active
 684 imino C=N bond. MnIMP and MnIPIMP are relatively
 685 unhindered, and the catalytic behaviors are almost identical.
 686 The initial reduction of parent and/or the cationic aqua
 687 complex results in the formation of the two-electron-reduced
 688 five-coordinate anion that reacts efficiently with CO₂; no dimer
 689 is observed during the reduction of MnIMP (Figure 10) or
 690 MnIPIMP (Figure 11).

691 The catalytic process at the initial cathodic wave is, however,
 692 inhibited by the rapid formation of a stable bicarbonate
 693 complex, absorbing at 2036, 1940, 1924, and 1671 cm⁻¹ for the
 694 IPIMP species, in line with the reports for sterically hindered
 695 Mn-mesityl-bipyridine²⁵ complexes and Mn-R-DAB com-
 696 plexes.⁸ A further negative potential shift of ca. 0.7 V is needed
 697 to reduce the bicarbonate complex, resulting in the recovery of
 698 the five-coordinate anion that triggers the catalytic conversion
 699 of CO₂.

700 For the nonhindered IMP and IPIMP ligands the five-
 701 coordinate anion reacts rapidly and is not observed in the IR
 702 spectra on this time scale (for IMP) and only at a low
 703 concentration (for IPIMP). The production of CO in the thin
 704 solution layer results in the displacement of the α -diimine
 705 ligand in the five-coordinate anion, forming the pentacarbonyl
 706 species [Mn(CO)₅]⁻ clearly seen in the IR spectra via the
 707 growth of bands at 1897 and 1865 cm⁻¹ (species C in Figures
 708 10–13). Remarkably, in these two cases only a comparatively

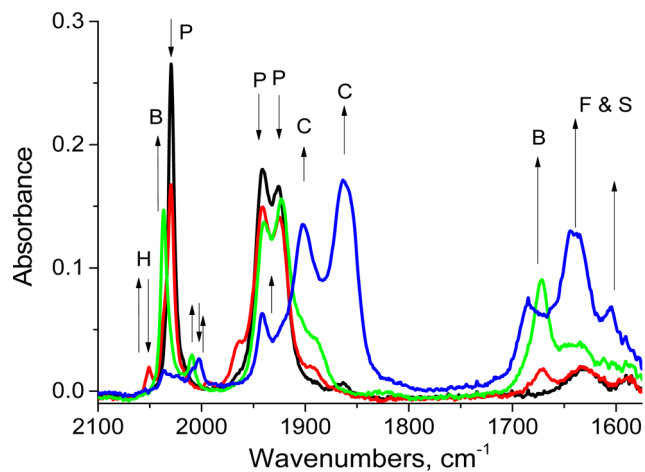


Figure 10. IR spectral changes accompanying in situ reduction of MnIMP ([MnBr(CO)₃(IMP)]) in CO₂-saturated acetonitrile/0.2 M [Bu₄N][PF₆] within an OTTLE cell: (P) [MnBr(CO)₃(IMP)]; (B) [Mn(CO)₃(IMP)(η^1 -OCO₂H)]; (C) [Mn(CO)₅]⁻; (H) [Mn(CO)₃(H₂O)(IMP)]⁺; (F and S) free bicarbonate (OCO₂H⁻) and subordinate formate (OCHO⁻) accompanying the catalytic reduction of CO₂ to CO.

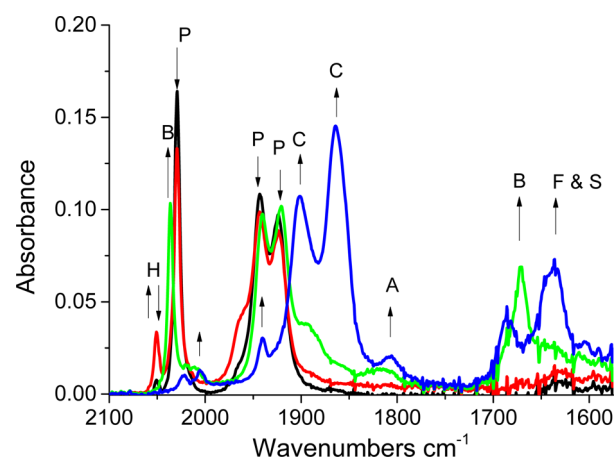


Figure 11. IR spectral changes accompanying in situ reduction of MnIPIMP ([MnBr(CO)₃(IPIMP)]) in CO₂-saturated acetonitrile/0.2 M [Bu₄N][PF₆] in an OTTLE cell: (P) [MnBr(CO)₃(IPIMP)]; (A) [Mn(CO)₃(IPIMP)]⁻; (B) [Mn(CO)₃(IPIMP)(η^1 -OCO₂H)]; (C) [Mn(CO)₅]⁻; (H) [Mn(CO)₃(H₂O)(IPIMP)]⁺; (F and S) free bicarbonate (OCO₂H⁻) and subordinate formate (OCHO⁻) accompanying the catalytic reduction of CO₂ to CO.

small amount of free bicarbonate or free formate (1685, 1638, 709
 and 1604 cm⁻¹ for the IPIMP species) relative to [Mn(CO)₅]⁻ 710
 is observed, marking the high catalytic efficiency toward CO 711
 production. 712

Upon reduction of the more C=N hindered DIPIMP 713
 complex, the five-coordinate anion formed does not react with 714
 CO₂ efficiently and a metastable population of the anionic five- 715
 coordinate MnDIPIMP species [Mn(CO)₃(DIPIMP)]⁻ is 716
 detected even under a high excess of CO₂. Interestingly, and 717
 differently from the other complexes in the Mn-IP series, the 718
 formation of a bicarbonate complex is only detected at the 719
 potential corresponding to the reduction of CO₂-associated 720
 species at around -2 V vs Fc/Fc⁺, while on prior coordination 721
 of CO₂ to the five-coordinate anion at the parent MnDIPIMP 722
 cathodic wave no bicarbonate ligand signature is detected. At 723
 the catalytic potential where the bicarbonate complex is 724

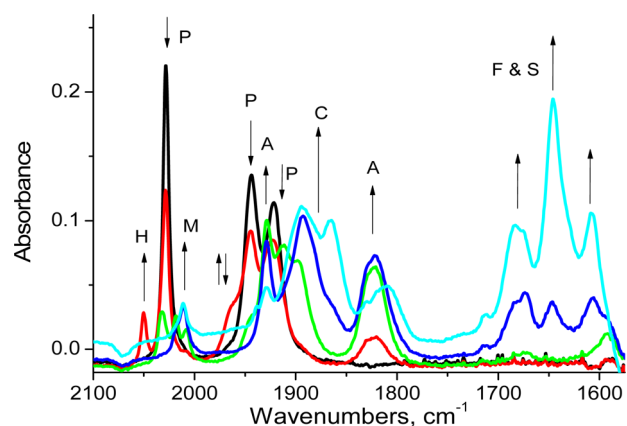


Figure 12. IR spectral changes accompanying in situ reduction of MnDIPIMP in CO₂-saturated acetonitrile/0.2 M [Bu₄N][PF₆] within an OTTLE cell: (P) [MnBr(CO)₃(DIPIMP)]; (A) [Mn(CO)₃(DIPIMP)]⁻; (B) [Mn(CO)₃(DIPIMP)(η¹-OCO₂H)]; (H) aqua complex [Mn(CO)₃(H₂O)(DIPIMP)]⁺; (C) [Mn(CO)₅]⁻; (M) [Mn(CO)₃(MeCN)(DIPIMP)]⁺; (F and S) free bicarbonate (OCO₂H⁻) and subordinate formate (OCHO⁻).

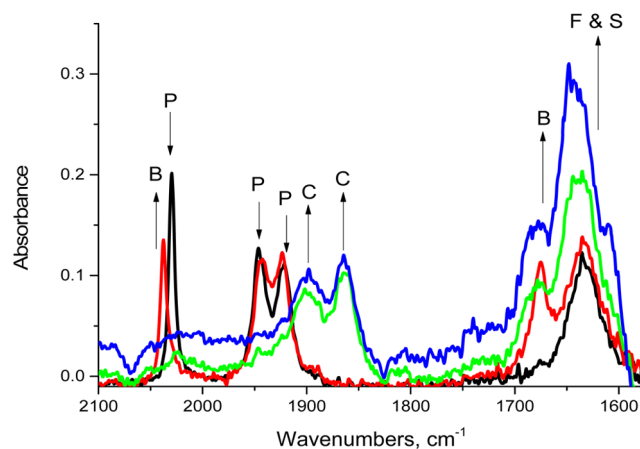
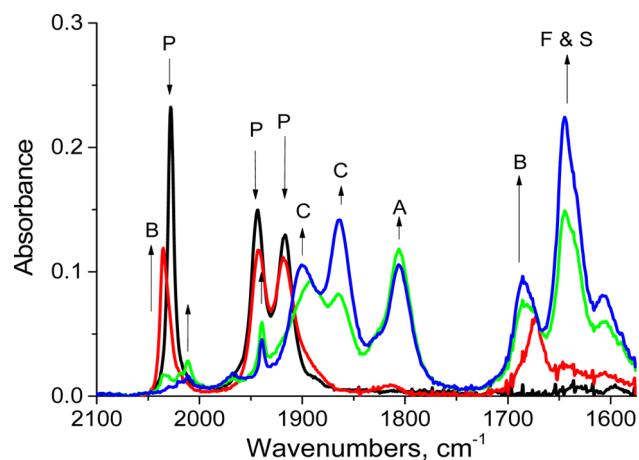


Figure 13. IR spectral changes accompanying in situ reduction of complexes in CO₂-saturated acetonitrile/0.2 M [Bu₄N][PF₆] within an OTTLE cell. (top) For MnTBIEP: (P) [MnBr(CO)₃(TBIEP)]; (A) [Mn(CO)₃(TBIEP)]⁻; (B) [Mn(CO)₃(TBIEP)(η¹-OCO₂H)]; (C) [Mn(CO)₅]⁻; (F and S) free bicarbonate (OCO₂H⁻) and formate (OCHO⁻) accompanying the catalytic reduction of CO₂ to CO. (bottom) For MnTBIMP: (P) [MnBr(CO)₃(TBIMP)]; (B) [Mn(CO)₃(TBIMP)(η¹-OCO₂H)]; (C) [Mn(CO)₅]⁻; (F and S) free bicarbonate (OCO₂H⁻) and formate (OCHO⁻) accompanying the catalytic reduction of CO₂ to CO.

725 reduced, the conversion of CO₂ to CO is also inefficient. A high
726 concentration of the five-coordinate anion is still seen,
727 converting slowly to [Mn(CO)₅]⁻ when the concentration of
728 CO increases; at the same time the production of free
729 bicarbonate (and free formate) is much higher in comparison
730 to the MnIMP and MnIPIMP cases, marking the low catalytic
731 efficiency toward CO production. Notably, the lower CO-
732 stretching band of [Mn(CO)₃(DIPIMP)]⁻ becomes shifted
733 from its standard position (1829/1822 cm⁻¹) to lower energy
734 (ca. 1810 cm⁻¹) at the advanced stage of the catalytic
735 conversion. This shift may indicate the presence of an
736 observable adduct of the five-coordinate anion, most likely
737 with CO₂ or formate (over the Mn–N=C bond). In this
738 context it is interesting to note that the related Re-IP complex³⁷
739 forms the carbonate complex in two 1e-reduction steps, via a
740 direct coordination to the Re center, without C=N being
741 directly involved.

742 In the case of MnTBIEP the imino C=N bond is hindered
743 both at the carbon atom via the methyl group and by the *tert*-
744 butyl group on the phenyl moiety. There are similarities with
745 but also differences from the hindered DIPIMP complex, which
746 does not have a hindering group at the C atom of the imino
747 C=N moiety. Upon reduction of the parent complex in CO₂-
748 saturated acetonitrile the five-coordinate anion [Mn-
749 (CO)₃(TBIEP)]⁻ coordinates CO₂, forming the bicarbonate
750 complex readily (similar to IMP and IPIMP) with the
751 characteristic IR absorption band at 1673 cm⁻¹.^{8,30}

752 A small amount of the five-coordinate anion [Mn-
753 (CO)₃(TBIEP)]⁻ is observed in the initial step. Lowering the
754 potential to around -1.5 V vs Fc/Fc⁺ results in catalytic
755 conversion of the bicarbonate complex; however, similar to
756 MnDIPIMP this conversion is not efficient in comparison with
757 MnIMP and MnIPIMP. This is shown via the slower growth of
758 [Mn(CO)₅]⁻ in comparison to IPIMP and the greater
759 quantities of free bicarbonate produced. As with MnDIPIMP
760 the five-coordinate anion “adduct” form is observed with the
761 lower energy CO-stretching band shifted to a lower wave-
762 number (from 1814 to 1803 cm⁻¹). Thus, hindering the imine
763 C atom does not affect adduct formation between CO₂ and
764 [Mn(CO)₃(TBIEP)]⁻.

765 However, at the negative potentials where the bicarbonate
766 complex is reduced (recovering the catalytic five-coordinate
767 anion) the hindrance provided by the methyl and *tert*-butyl
768 groups also negatively affects the catalytic formation of CO₂ to
769 CO (as evidenced by large amounts of free bicarbonate and
770 slow formation of [Mn(CO)₅]⁻ at lower CO concentration). It
771 is not very clear whether this greater hindrance is due directly
772 to the presence of the methyl group on the C position or
773 whether this is due to the *tert*-butyl group inhibiting rotation
774 of the phenyl moiety and preventing the five-coordinate anion
775 from adopting a more suitable (pyramidal) geometry for CO₂
776 association.

777 Again, MnTBIMP behaves in a fashion similar to that of
778 MnTBIEP. Upon reduction the parent complex rapidly
779 associates CO₂, forming the bicarbonate complex; as the
780 reduction potential is lowered further, the bicarbonate complex
781 is reduced, forming CO which is able to displace the TBIMP
782 and forming [Mn(CO)₅]⁻. One important difference is that
783 significantly less (if any) five-coordinate anion is observed in
784 the presence of CO₂ than was the case with both MnTBIEP

785 and MnDIPIMP. This suggests that ^tBu is not as sterically
786 demanding as two ⁱPr groups in these systems, as CO₂ is still
787 able to coordinate.

788 **Estimation of Electrocatalytic Activity toward CO**
789 **Production using Gas Chromatography.** The CO
790 concentration as a function of time in the course of controlled
791 potential electrolysis estimated by GC analysis of the headspace
792 of the electrolysis cell shows a gradual buildup of CO in the
793 course of the electrolysis (Figure S119 in the Supporting
794 Information). A comparison with the performance of [MnBr-
795 (CO)₃(bpy)] catalyst investigated under identical conditions
796 (see Figure S19) shows that the efficiency of CO production
797 for the new catalysts 1–5 is comparable to that of
798 [MnBr(CO)₃(bpy)], with the least sterically hindered
799 MnIMP complex being somewhat more efficient. Due to the
800 large volumes used in the experiment, considerable secondary
801 processes occur during bulk electrolysis, manifested in the loss
802 of the initial intense yellow-red color of the solution as the
803 reaction progressed, which was concomitant with an increase in
804 current toward the end of the electrolysis. These deviations
805 from an ideal behavior suggest that, as CO₂ is depleted in
806 solution, competing catalyst degradation pathways begin to
807 occur, precluding reliable estimates of efficiencies.

808 Estimation of efficiency from the CV data was done by the
809 relative $i_{\text{cat}}/i_{\text{p}}$ values (Table S1 in the Supporting Information)
810 following the method described in refs 4 and 7. Comparing the
811 current values detected in the CV at -2.24 V (vs Fc/Fc⁺)
812 recorded under a CO₂ and N₂ atmosphere in acetonitrile/water
813 also shows that the performances of 1–5 are comparable to one
814 another and are comparable to that of [Mn(CO)₃(bpy)Br], at
815 30–60% efficiency. It is important that the most sterically
816 protected complexes, MnDIPIMP and MnTBIEP, seem to be
817 performing better as far as $i_{\text{cat}}/i_{\text{p}}$ values are concerned but that
818 the least sterically hindered complex, MnIMP, is the most
819 efficient in the series. These observations are different from the
820 observation of MnTBIMP producing more CO than [Mn-
821 (bpy)(CO)₃Br] in the bulk electrolysis/GC experiments. While
822 these data can only be considered in relative terms, they do
823 show the potential of these complexes to act as a test bed for
824 optimizing steric vs electronic effects in CO₂ reduction,
825 whereby the thermodynamic factors, the rate of CO₂
826 coordination, and the rate of decomposition of catalyst
827 precursor species need to be balanced.

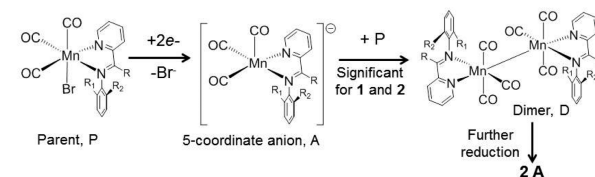
828 The main transformation pathways of 1–5 upon reduction
829 under an inert atmosphere, and under an atmosphere of CO₂,
830 are summarized schematically in Figure 14.

831 CONCLUSIONS

832 A series of Mn(I) tricarbonyl electrocatalysts for CO₂ reduction
833 which employ, for the first time, asymmetric α -diimine ligands,
834 imino-pyridines, has been developed, and their catalytic activity
835 has been confirmed and evaluated in detail.

836 We have demonstrated through conventional and thin-layer
837 cyclic voltammetry, UV–vis and IR spectroscopy, and DFT
838 computational analysis the π decoupling of the phenyl from the
839 Mn(pyridine-CCN) metallacycle. The practical effect of this
840 feature is the ability to disentangle steric and electronic effects
841 of the α -diimine ligand on the catalytic properties. Until now,
842 introduction of sterically bulky groups, which are also typically
843 electron donating, was coming at the price of an increased
844 overpotential required for CO₂ reduction. The use of an
845 asymmetric α -diimine has allowed us to probe the effect of
846 adding ever greater sterically demanding groups without much

(a) inert atmosphere



(b) CO₂ atmosphere

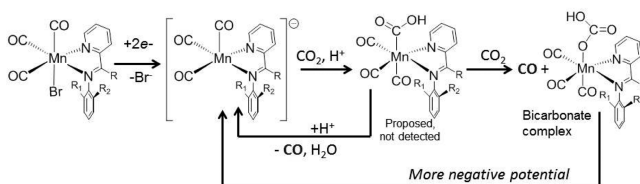


Figure 14. Main transformation pathways of 1–5 upon reduction under (a) an inert atmosphere and (b) an atmosphere of CO₂. A is detected for 3 only due to the comparatively slower reaction of [3][−] with CO₂.

change in the catalytic potential. We have demonstrated that a
systematic increase in the steric hindrance of the R₁ and R₂
groups in the IMP subseries results in the switch of the nature
of the first reduction product detected on the time scale of the
experiment under an inert gas atmosphere, from a dimer to a
five-coordinate anion, at a very similar reduction potential. In
the absence of sterically hindering groups on the phenyl ring,
MnIMP, a dimer is formed, while increasing the steric
hindrance by adding ^tPr groups to the R₁ and R₂ positions
(MnDIPIMP) resulted in direct formation of the five-
coordinate anion, in line with prior observations for similar
sterically hindered ligands.^{23,26} MnIPIMP (in which case the
dimer may be reduced at the parent cathodic wave due to
slightly negatively shifted reduction potential vs that for
MnIMP) exhibited behavior intermediate to that of MnIMP
and MnDIPIMP with both the dimer and the five-coordinate
anion observed to be formed concurrently. MnTBIMP and
MnTBIEP both formed the five-coordinate anion directly upon
reduction of the parent complex.

Under a CO₂ atmosphere, all of the complexes reduce CO₂
to CO. The buildup of CO in the thin-layer spectroelectro-
chemical cell resulted in the displacement of the α -diimine
ligand, forming [Mn(CO)₅][−]. The complex containing the
most sterically demanding ligand, DIPIMP, is as anticipated
least susceptible to α -diimine displacement with CO, forming
exclusively the five-coordinate anion upon the first reduction;
it also has the least propensity to coordinate CO₂, resulting in a
considerable buildup of the concentration of the five-coordinate
anion. An intermediate formation of the bicarbonate is also
likely, as a band at 1686 cm^{−1} is present at intermediate times.
Of particular interest is that the least sterically hindered
complex, MnIMP, seemed to form a CO₂-associated complex
directly upon the first reduction, with no significant formation
of the dimer being observed on the time scale of the
experiment. This behavior is similar to that reported for the
symmetric nonaromatic Mn-R-DAB (R = alkyl) compounds.^{8,30}
The formation of a stable bicarbonate complex, either through
the coordination to the metal center or via the imino C=N
bond,^{23,37} leads to the need for increased overpotential. From
that point of view, the steric hindering (protection) of the
metal center/the imino C=N bond in the Mn(IP) complexes
is advantageous, as it disfavors the Mn–Mn dimerization (when

889 MnIMP is compared with MnDIPIMP). However, such steric
890 crowding also slows the catalytic conversion of CO₂ to CO at
891 the negative overpotentials, as can be seen in the GC data and
892 from the i_{cat}/i_p values. A difference in the reactivity of
893 MnTBIMP and MnTBIEP, where no dimer formation has
894 been detected for either of the complexes in the IR-SEC
895 experiments but where MnTBIEP exhibits slower CO₂
896 conversion due to R = CH₃, alters the HOMO–LUMO gap
897 in comparison to the IMP series as well as introduces additional
898 steric bulk, further supporting the notion that it is possible to
899 separate steric and electronic factors to a large extent. Balancing
900 these factors by careful ligand design may lead to the optimal
901 solution.

902 The new family of CO₂ reduction catalysts presents an
903 exciting platform for versatile and relatively independent tuning
904 of steric and electronic properties, offering a far greater
905 tunability in comparison to catalysts with aromatic bpy-based or
906 nonaromatic R-DAB-based ligands and abundant options to
907 refine and optimize Mn tricarbonyl CO₂ reduction catalysts.

908 ■ ASSOCIATED CONTENT

909 ● Supporting Information

910 The Supporting Information is available free of charge on the
911 ACS Publications website at DOI: 10.1021/acs.inorg-
912 chem.6b01477.

913 Calculated frontier orbitals from HOMO-3 to LUMO+3
914 for all studied complexes, complete CV measurements,
915 control experiments, crystallographic data, and ¹H NMR
916 spectra of the new complexes (PDF)

917 Crystallographic data (CIF)

918 Crystallographic data (CIF)

919 ■ AUTHOR INFORMATION

920 Corresponding Authors

921 *E-mail for F.H.: F.Hartl@reading.ac.uk.

922 *E-mail for J.A.W.: Julia.Weinstein@sheffield.ac.uk.

923 ORCID

924 Anthony J. H. M. Meijer: 0000-0003-4803-3488

925 Julia A. Weinstein: 0000-0001-6883-072X

926 Notes

927 The authors declare no competing financial interest.

928 ■ ACKNOWLEDGMENTS

929 The authors are grateful to E. J. Carrington, T. M. Roseveare,
930 and C. M. Kiker for assistance in interpreting the X-ray
931 diffraction data, Drs. A. Haynes and S. Parker for discussions,
932 and G. Chandrakumar for experimental assistance. Support of
933 the University of Sheffield and its SURE scheme, Shine DTC,
934 the University of Reading (Project D14-015), the EPSRC, and
935 the RSC Undergraduate Bursary (T.K. and H.F.) is gratefully
936 acknowledged.

937 ■ REFERENCES

938 (1) Morris, A. J.; Meyer, G. J.; Fujita, E. Molecular Approaches to the
939 Photocatalytic Reduction of Carbon Dioxide for Solar Fuels. *Acc.*
940 *Chem. Res.* **2009**, *42*, 1983–1994.

941 (2) Bourrez, M.; Molton, F.; Chardon-Noblat, S.; Deronzier, A.
942 [Mn(bipyridyl)(CO)₃Br]: An Abundant Metal Carbonyl Complex as
943 Efficient Electrocatalyst for CO₂ Reduction. *Angew. Chem., Int. Ed.*
944 **2011**, *50*, 9903–9906.

(3) Hawecker, J.; Lehn, J.-M.; Zissel, R. Electrocatalytic Reduction
945 of Carbon Dioxide Mediated by Re(bipy)(CO)₃Cl (bipy = 2,2'-
946 bipyridine). *J. Chem. Soc., Chem. Commun.* **1984**, 328–330.

(4) Smieja, J. M.; Benson, E. E.; Kumar, B.; Grice, K. A.; Seu, C. S.;
948 Miller, A. J. M.; Mayer, J. M.; Kubiak, C. P. Kinetic and structural
949 studies, origins of selectivity, and interfacial charge transfer in the
950 artificial photosynthesis of CO. *Proc. Natl. Acad. Sci. U. S. A.* **2012**, *109*,
951 15646–15650.

(5) Grice, K. A.; Kubiak, C. P.; Aresta, M. Recent Studies of Rhenium
953 and Manganese Bipyridine Carbonyl Catalysts for the Electrochemical
954 Reduction of CO₂. *Adv. Inorg. Chem.* **2014**, *66*, 163–188. Aresta, M.;
955 Dibenedetto, A.; Angelini, A. Converting "Exhaust" Carbon into
956 "Working" Carbon. *Adv. Inorg. Chem.* **2014**, *66*, 259–288.

(6) Wong, K.; Chung, W.; Lau, C. The effect of weak Brønsted acids
958 on the electrocatalytic reduction of carbon dioxide by a rhenium
959 tricarbonyl bipyridyl complex. *J. Electroanal. Chem.* **1998**, *453*, 161–
960 170.

(7) Smieja, J. M.; Sampson, M. D.; Grice, K. A.; Benson, E. E.;
962 Froehlich, J. D.; Kubiak, C. P. Manganese as a Substitute for Rhenium
963 in CO₂ Reduction Catalysts: The Importance of Acids. *Inorg. Chem.*
964 **2013**, *52*, 2484–2491.

(8) Zeng, Q.; Tory, J.; Hartl, F. Electrocatalytic Reduction of Carbon
966 Dioxide with a Manganese(I) Tricarbonyl Complex Containing a
967 Nonaromatic α -Diimine Ligand. *Organometallics* **2014**, *33*, 5002–
968 5008.

(9) Rossenaar, B. D.; Hartl, F.; Stufkens, D. J.; Amatore, C.;
970 Maisonhaute, E.; Verpeaux, J.-N. Electrochemical and IR/UV-Vis
971 Spectroelectrochemical Studies of fac-[Mn(X)(CO)₃(Pr-DAB)]ⁿ (n
972 = 0, X = Br, Me, Bz; n = +1, X = THF, MeCN, nPrCN, P(OMe)₃; iPr-
973 DAB = 1,4-Diisopropyl-1,4-diaza-1,3-butadiene) at Variable Temper-
974 atures: Relation between Electrochemical and Photochemical Gen-
975 eration of [Mn(CO)₃(α -diimine)]⁻. *Organometallics* **1997**, *16*, 4675–
976 4685.

(10) Grills, D. C.; Farrington, J. A.; Layne, B. H.; Lyman, S. V.; Mello,
978 B. A.; Preses, J. M.; Wishart, J. F. Mechanism of the Formation of a
979 Mn-Based CO₂ Reduction Catalyst Revealed by Pulse Radiolysis with
980 Time-Resolved Infrared Detection. *J. Am. Chem. Soc.* **2014**, *136*,
981 5563–5566.

(11) Johnson, F. P. A.; George, M. W.; Hartl, F.; Turner, J. J.
983 Electrocatalytic Reduction of CO₂ Using the Complexes [Re(bpy)
984 (CO)₃L]ⁿ (n = +1, L = P(OEt)₃, CH₃CN; n = 0, L = Cl⁻, Otf⁻; bpy =
985 2,2'-Bipyridine; Otf⁻ = CF₃SO₃) as Catalyst Precursors: Infrared
986 Spectroelectrochemical Investigation. *Organometallics* **1996**, *15*, 3374–
987 3387.

(12) Smieja, J. M.; Kubiak, C. P. Re(bipy-Bu)(CO)₃Cl-improved
989 Catalytic Activity for Reduction of Carbon Dioxide: IR-Spectroelec-
990 trochemical and Mechanistic Studies. *Inorg. Chem.* **2010**, *49*, 9283–
991 9289.

(13) Machan, C. W.; Sampson, M. D.; Chabolla, S. A.; Dang, T.;
993 Kubiak, P. Developing a Mechanistic Understanding of Molecular
994 Electrocatalysts for CO₂ Reduction using Infrared Spectroelectro-
995 chemistry. *Organometallics* **2014**, *33*, 4550–4559.

(14) Cabeza, J. A.; Garcia-Alvarez, P.; Gobetto, R.; Gonzalez-Alvarez,
997 L.; Nervi, C.; Perez-Carreno, E.; Polo, D. [MnBrL(CO)₄] (L =
998 Amidinatogermylene): Reductive Dimerization, Carbonyl Substitution,
999 and Hydrolysis Reactions. *Organometallics* **2016**, *35*, 1761–1770.

(15) Machan, C. W.; Stanton, C. J.; Vandezande, J. E.; Majetich, G.
1001 F.; Schaefer, H. F.; Kubiak, C. P.; Agarwal, J. Electrocatalytic
1002 Reduction of Carbon Dioxide by Mn(CN)(2,2'-bipyridine)(CO)₃:
1003 CN Coordination Alters Mechanism. *Inorg. Chem.* **2015**, *54*, 8849–
1004 8856.

(16) Sieh, D.; Kubiak, C. P. A Series of Diamagnetic Pyridine
1006 Monoimine Rhenium Complexes with Different Degrees of Metal-to-
1007 Ligand Charge Transfer: Correlating ¹³C NMR Chemical Shifts with
1008 Bond Lengths in Redox-Active Ligands. *Chem. - Eur. J.* **2016**, *22*,
1009 10638–10650.

(17) Riplinger, C.; Sampson, M. D.; Ritzmann, A. M.; Kubiak, C. P.;
1011 Carter, E. A. Mechanistic Contrasts between Manganese and Rhenium
1012

- 1013 Bipyridine Electrocatalysts for the Reduction of Carbon Dioxide. *J.*
1014 *Am. Chem. Soc.* **2014**, *136*, 16285–16298.
- 1015 (18) Franco, F.; Cometto, C.; Ferrero Vallana, F.; Sordello, F.; Priola,
1016 E.; Minero, C.; Nervi, C.; Gobetto, R. A local proton source in a
1017 [Mn(bpy-R)(CO)₃Br]-type redox catalyst enables CO₂ reduction
1018 even in the absence of Brønsted acids. *Chem. Commun.* **2014**, *50*,
1019 14670–14673.
- 1020 (19) Bourrez, M.; Orio, M.; Molton, F.; Vezin, H.; Duboc, C.;
1021 Deronzier, A.; Chardon-Noblat, S. Pulsed-EPR Evidence of a
1022 Manganese(II) Hydroxycarbonyl Intermediate in the Electrocatalytic
1023 Reduction of Carbon Dioxide by a Manganese Bipyridyl Derivative.
1024 *Angew. Chem., Int. Ed.* **2014**, *53*, 240–243.
- 1025 (20) Sullivan, B. P.; Bolinger, C. M.; Conrad, D.; Vining, W. J.;
1026 Meyer, T. J. One- and Two-electron Pathways in the Electrocatalytic
1027 Reduction of CO₂ by *fac*-Re(bpy)(CO)₃Cl (bpy = 2,2'-bipyridine). *J.*
1028 *Chem. Soc., Chem. Commun.* **1985**, 1414–1416.
- 1029 (21) Stor, G. J.; Hartl, F.; van Outersterp, J. W. M.; Stufkens, D. J.
1030 Spectroelectrochemical (IR, UV/Vis) Determination of the Reduction
1031 Pathways for a Series of [Re(CO)₃(α -diimine)L']^{0/+} (L' = Halide,
1032 Otf⁻, THF, MeCN, *n*-PrCN, PPh₃, P(OMe)₃) Complexes. *Organo-*
1033 *metallics* **1995**, *14*, 1115–1131.
- 1034 (22) Walsh, J. J.; Smith, C. L.; Neri, G.; Whitehead, G. F. S.;
1035 Robertson, C. M.; Cowan, A. J. Improving the efficiency of
1036 electrochemical CO₂ reduction using immobilized manganese
1037 complexes. *Faraday Discuss.* **2015**, *183*, 147–160.
- 1038 (23) Stor, G. J.; Morrison, S. L.; Stufkens, D. J.; Oskam, A. The
1039 Remarkable Photochemistry of *fac*-XMn(CO)₃(α -diimine) (X =
1040 Halide): Formation of Mn₂(CO)₆(α -diimine)₂ via the *mer* Isomer
1041 and Photocatalytic Substitution of X⁻ in the Presence of PR₃.
1042 *Organometallics* **1994**, *13*, 2641–2650.
- 1043 (24) Sampson, M. D.; Kubiak, C. P. Electrocatalytic Dihydrogen
1044 Production by an Earth-Abundant Manganese Bipyridine Catalyst.
1045 *Inorg. Chem.* **2015**, *54*, 6674–6676.
- 1046 (25) Sampson, M. D.; Nguyen, A. D.; Grice, K. A.; Moore, C. E.;
1047 Rheingold, A. L.; Kubiak, C. P. Manganese Catalysts with Bulky
1048 Bipyridine Ligands for the Electrocatalytic Reduction of Carbon
1049 Dioxide: Eliminating Dimerization and Altering Catalysis. *J. Am. Chem.*
1050 *Soc.* **2014**, *136*, 5460–5471.
- 1051 (26) Agarwal, J.; Shaw, T. W.; Stanton, C. J., III; Majetich, G. F.;
1052 Bocarsly, A. B.; Schaefer, H. F., III NHC-Containing Manganese(I)
1053 Electrocatalysts for the Two-Electron Reduction of CO₂. *Angew. Chem.*
1054 **2014**, *126*, 5252–5255.
- 1055 (27) Costentin, C.; Robert, M.; Savéant, J.-M. Catalysis of the
1056 electrochemical reduction of carbon dioxide. *Chem. Soc. Rev.* **2013**, *42*,
1057 2423–2436.
- 1058 (28) Sampson, M. D.; Kubiak, C. P. Manganese Electrocatalysts with
1059 Bulky Bipyridine Ligands: Utilizing Lewis Acids To Promote Carbon
1060 Dioxide Reduction at Low Overpotentials. *J. Am. Chem. Soc.* **2016**,
1061 *138*, 1386–1393.
- 1062 (29) Lam, Y. C.; Nielsen, R. J.; Gray, H. B.; Goddard, W. A. A Mn
1063 Bipyrimidine Catalyst Predicted To Reduce CO₂ at Lower Over-
1064 potential. *ACS Catal.* **2015**, *5*, 2521–2528.
- 1065 (30) Vollmer, M. V.; Machan, C. W.; Clark, M. L.; Antholine, W. E.;
1066 Agarwal, J.; Schaefer, H. F.; Kubiak, C. P.; Walensky, J. R. Synthesis,
1067 Spectroscopy, and Electrochemistry of (α -Diimine)M(CO)₃Br, M =
1068 Mn, Re, Complexes: Ligands Isoelectronic to Bipyridyl Show
1069 Differences in CO₂ Reduction. *Organometallics* **2015**, *34*, 3–12.
- 1070 (31) Agarwal, J.; Shaw, T. W.; Schaefer, H. F., III; Bocarsly, A. B.
1071 Design of a Catalytic Active Site for Electrochemical CO₂ Reduction
1072 with Mn(I) Tri-carbonyl Species. *Inorg. Chem.* **2015**, *54*, 5285–5294.
- 1073 (32) Stufkens, D. J.; van Outersterp, J. W. M.; Oskam, A.; Rossenaar,
1074 B. D.; Stor, G. J. The photochemical formation of organometallic
1075 radicals from α -diimine complexes having a metal-metal, metal-alkyl or
1076 metal-halide bond. *Coord. Chem. Rev.* **1994**, *132*, 147–154.
- 1077 (33) Rossenaar, B. D.; Kleverlaan, C. J.; van der Ven, M. C. E.;
1078 Stufkens, D. J.; Oskam, A.; Fraanje, J.; Goubitz, K. Synthesis and
1079 spectroscopic properties of Re(R)(CO)₃(α -diimine) (R = alkyl; α -
1080 diimine = R'-pyCa, R'-DAB) complexes. Crystal structure of Re(Me)
1081 (CO)₃(^tPr-DAB). *J. Organomet. Chem.* **1995**, *493*, 153–162.
- (34) Sieh, D.; Lacy, D. C.; Peters, J. C.; Kubiak, C. P. Reduction of
CO₂ by Pyridine Monoimine Molybdenum Carbonyl Complexes: Cooperative
Metal–Ligand Binding of CO₂. *Chem. - Eur. J.* **2015**, *21*, 8497–8503.
- (35) Gonsalvi, L.; Gaunt, J. A.; Adams, H.; Castro, A.; Sunley, G. J.;
Haynes, A. Quantifying Steric Effects of α -Diimine Ligands. Oxidative
Addition of MeI to Rhodium(I) and Migratory Insertion in
Rhodium(III) Complexes. *Organometallics* **2003**, *22*, 1047–1054.
- (36) Machan, C. W.; Chabolla, S. A.; Kubiak, C. P. Reductive
Disproportionation of Carbon Dioxide by an Alkyl-Functionalized
Pyridine Monoimine Re(I) *fac*-Tricarbonyl Electrocatalyst. *Organo-*
metallics **2015**, *34*, 4678–4683.
- (37) Alvarez, C. M.; García-Rodríguez, R.; Miguel, D. Carbonyl
complexes of manganese, rhenium and molybdenum with ethynylimino-
pyridine ligands. *J. Organomet. Chem.* **2007**, *692*, 5717–5726.
- (38) Alvarez, C. M.; García-Rodríguez, R.; Miguel, D. Pyridine-2-
carboxaldehyde as ligand: Synthesis and derivatization of carbonyl
complexes. *Dalton Trans.* **2007**, 3546–3554.
- (39) Bond, M.; Grabaric, B. S.; Grabaric, Z. Kinetic and
Thermodynamic Study of Reactions of Some Substituted Manganese-
(I) and Manganese(II) Tricarbonyl Complexes Using Spectrophotometric
and Electrochemical Techniques. *Inorg. Chem.* **1978**, *17*, 1013–
1018.
- (40) Krause, L.; Herbst-Irmer, R.; Sheldrick, G. M.; Stalke, D.
Comparison of silver and molybdenum microfocus X-ray sources for
single-crystal structure determination. *J. Appl. Crystallogr.* **2015**, *48*, 3–
10.
- (41) Frisch, M. J.; Trucks, G. W.; Schlegel, H. B.; Scuseria, G. E.;
Robb, M. A.; Cheeseman, J. R.; Scalmani, G.; Barone, V.; Mennucci,
B.; Petersson, G. A.; Nakatsuji, H.; Caricato, M.; Li, X.; Hratchian, H.
P.; Izmaylov, A. F.; Bloino, J.; Zheng, G.; Sonnenberg, J. L.; Hada, M.;
Ehara, M.; Toyota, K.; Fukuda, R.; Hasegawa, J.; Ishida, M.; Nakajima,
T.; Honda, Y.; Kitao, O.; Nakai, H.; Vreven, T.; Montgomery, J. A., Jr.;
Peralta, J. E.; Ogliaro, F.; Bearpark, M.; Heyd, J. J.; Brothers, E.; Kudin,
K. N.; Staroverov, V. N.; Kobayashi, R.; Normand, J.; Raghavachari, K.;
Rendell, A.; Burant, J. C.; Iyengar, S. S.; Tomasi, J.; Cossi, M.; Rega,
N.; Millam, J. M.; Klene, M.; Knox, J. E.; Cross, J. B.; Bakken, V.;
Adamo, C.; Jaramillo, J.; Gomperts, R.; Stratmann, R. E.; Yazyev, O.;
Austin, A. J.; Cammi, R.; Pomelli, C.; Ochterski, J. W.; Martin, R. L.;
Morokuma, K.; Zakrzewski, V. G.; Voth, G. A.; Salvador, P.;
Dannenberg, J. J.; Dapprich, S.; Daniels, A. D.; Farkas, Ö.;
Foresman, J. B.; Ortiz, J. V.; Cioslowski, J.; Fox, D. J. *Gaussian 09*,
Revision D.01; Gaussian, Inc., Wallingford, CT, 2013.
- (42) Becke, A. D. Density-functional thermochemistry. III. The role
of exact exchange. *J. Chem. Phys.* **1993**, *98*, 5648–5652.
- (43) Lee, C.; Yang, W.; Parr, R. G. Development of the Colle-Salvetti
correlation-energy formula into a functional of the electron density.
Phys. Rev. B: Condens. Matter Mater. Phys. **1988**, *37*, 785–789.
- (44) Nicklass, A.; Dolg, M.; Stoll, H.; Preuss, H. Ab initio energy-
adjusted pseudopotentials for the noble gases Ne through Xe: Calculation
of atomic dipole and quadrupole polarizabilities. *J. Chem. Phys.*
1995, *102*, 8942–8952.
- (45) Dunning, T. H., Jr.; Hay, P. J. In *Modern Theoretical Chemistry*;
Schaefer, H. F., Ed.; Plenum Press: New York, 1977; Vol. 3.
- (46) Krishnan, R.; Binkley, J. S.; Seeger, R.; Pople, J. A. Self-
consistent molecular orbital methods. XX. A basis set for correlated
wave functions. *J. Chem. Phys.* **1980**, *72*, 650–654.
- (47) McLean, A. D.; Chandler, G. S. Contracted Gaussian basis sets
for molecular calculations. I. Second row atoms, Z = 11–18. *J. Chem. Phys.*
1980, *72*, 5639–5648.
- (48) Mennucci, B.; Tomasi, J. Continuum solvation models: A new
approach to the problem of solute's charge distribution and cavity
boundaries. *J. Chem. Phys.* **1997**, *106*, 5151–5158.
- (49) Cossi, M.; Barone, V.; Mennucci, B.; Tomasi, J. Ab initio study
of ionic solutions by a polarizable continuum dielectric model. *Chem. Phys. Lett.*
1998, *286*, 253–260.
- (50) Bistoni, G.; Rampino, S.; Scafuri, N.; Ciancaleoni, G.; Zuccaccia,
D.; Belpassi, L.; Tarantelli, F. How π back-donation quantitatively

1150 controls the CO stretching response in classical and non-classical
1151 metal carbonyl complexes. *Chem. Sci.* **2016**, *7*, 1174–1184.